Journal of Computational Physics **175,** 645–673 (2002)
doi:10.1006/jcph.2001.6961, available online at http://www.idealibrary.com on IDEAL®

Hyperbolic Divergence Cleaning for the MHD Equations

A. Dedner,* F. Kemm,† D. Kröner,* C.-D. Munz,† T. Schnitzer,* and M. Wesenberg*

**Institut für Angewandte Mathematik, Universität Freiburg, Freiburg, Germany; and †Institut für Aerodynamik und Gasdynamik, Universität Stuttgart, Stuttgart, Germany*
E-mail: kemm@iag.uni-stuttgart.de, munz@iag.uni-stuttgart.de, dedner@mathematik.uni-freiburg.de, dietmar@mathematik.uni-freiburg.de, schnitz@mathematik.uni-freiburg.de, and wesenber@mathematik.uni-freiburg.de

Received April 3, 2001; revised October 15, 2001

In simulations of magnetohydrodynamic (MHD) processes the violation of the divergence constraint causes severe stability problems. In this paper we develop and test a new approach to the stabilization of numerical schemes. Our technique can be easily implemented in any existing code since there is no need to modify the solver for the MHD equations. It is based on a modified system in which the divergence constraint is coupled with the conservation laws by introducing a generalized Lagrange multiplier. We suggest a formulation in which the divergence errors are transported to the domain boundaries with the maximal admissible speed and are damped at the same time. This corrected system is hyperbolic and the density, momentum, magnetic induction, and total energy density are still conserved. In comparison to results obtained without correction or with the standard "divergence source terms," our approach seems to yield more robust schemes with significantly smaller divergence errors.

Key Words: MHD equations; finite-volume schemes; divergence cleaning.

1. INTRODUCTION

Electrically conducting fluid flow in which the electromagnetic forces can be of the same order or even greater than the hydrodynamic ones is often modeled by the equations of magnetohydrodynamics (MHD). The ideal MHD equations consist of a set of nonlinear hyperbolic equations,

$$\partial_t \rho + \nabla \cdot (\rho \mathbf{u}) = 0, \tag{1a}$$

$$\partial_t (\rho \mathbf{u}) + \nabla \cdot \left[\rho \mathbf{u}\mathbf{u}^T + \left(p + \frac{1}{2}|\mathbf{B}|^2 \right) \mathcal{I} - \mathbf{B}\mathbf{B}^T \right] = 0, \tag{1b}$$

0021-9991/02 $35.00

$$\partial_t \mathbf{B} + \nabla \cdot (\mathbf{u}\mathbf{B}^T - \mathbf{B}\mathbf{u}^T) = 0, \tag{1c}$$

$$\partial_t e + \nabla \cdot \left[\left(e + p + \frac{1}{2}|\mathbf{B}|^2 \right) \mathbf{u} - \mathbf{B}(\mathbf{u} \cdot \mathbf{B}) \right] = 0, \tag{1d}$$

together with the additional divergence constraint

$$\nabla \cdot \mathbf{B} = 0. \tag{2}$$

Here $\mathbf{B} = (B_x, B_y, B_z)^T$ denotes the magnetic induction, $\mathbf{u} = (u_x, u_y, u_z)^T$ the fluid velocity, ρ the density, and e the energy density. The hydrodynamic pressure p is given by the equation of state for a perfect gas,

$$p = (\gamma - 1) \left(e - \frac{1}{2}\rho|\mathbf{u}|^2 - \frac{1}{2}|\mathbf{B}|^2 \right), \tag{3}$$

with adiabatic exponent $\gamma > 1$. This system combines the equations of gas dynamics with the Maxwell equations for problems in which relativistic, viscous, and resistive effects can be neglected; the permeability is set to unity. If the initial data for the magnetic field satisfy (2), then an exact solution will satisfy this constraint for all times. For smooth solutions this is directly obtained from the evolution equations for the magnetic field (1c), because they can be written in the equivalent form $\partial_t \mathbf{B} + \nabla \times (\mathbf{B} \times \mathbf{u}) = 0$ and we have $\nabla \cdot (\nabla \times \cdot) \equiv 0$. Hence numerical methods are usually based only on the hyperbolic evolution equations (1a)–(1d).

Because usually the discrete divergence of the discrete curl is not exactly zero, $\nabla \cdot \mathbf{B}$ errors arise in numerical simulations and may increase with time. If this happens, the behavior of the system can become unphysical: Magnetic field lines may have wrong topologies, leading to plasma transport *orthogonal* to the magnetic field. This effect is discussed by Brackbill and Barnes [12], Brackbill [11], and Balsara and Spicer [6].

Schemes have been developed which imitate the analytical fact that the divergence of a curl equals zero. These schemes are often referred to as "constrained transport methods." The first scheme of this type was proposed by Yee [46] for the Maxwell equations. Generalizations were introduced by Holland [26] and by Madsen and Ziolkowski [30]. This approach has been adapted to the MHD equations by Brecht *et al.* [13], Evans and Hawley [22], Stone and Norman [41], and DeVore [21]. Recent enhancements can be found in [6, 18, 29, 39, 43]. The main idea of the constrained transport approach is to use a special discretization of the magnetic field equations. This means that the underlying base scheme is only partially used and thus some of its desired properties may be lost. Moreover, these schemes are restricted to structured grids and require large stencils for the spatial discretization (cf. [43, p. 646]).

In recent years upwind finite-volume schemes, such as Godunov-type schemes or flux-vector-splitting schemes, have become very popular in numerical gas dynamics. This is due to the fact that by using this approach one can obtain discrete shock profiles without generating spurious oscillations as well as second- or higher-order accuracy in smooth parts of the flow. Among the first to apply Godunov-type schemes to the MHD equations were Brio and Wu [14]. Recent examples include those in [7, 9, 15, 16, 19, 20, 37, 38, 45, 48].

In the finite-volume approach each component of the curl of a vector field is interpreted as the divergence of a flux and integrated using Gauss' theorem. In many implementations

a discrete divergence applied to the discrete curl will give zero only in an approximate way. Therefore, to prevent divergence errors from increasing with time, some correction technique has to be added to these schemes. A well-known correction method is the projection of the magnetic field into the space of divergence-free vector fields, also known as "Hodge projection." This method was implemented among others by Balsara [4, 5], who discretized the Laplace operator in Fourier space. Furthermore, in the finite-volume approach the numerical fluxes between adjacent grid cells are usually calculated by considering the one-dimensional wave propagation in the normal direction of the grid face. In this one-dimensional setting, condition (2) means that there is no jump in the normal component of the magnetic field across the interface. In multidimensional simulations this constraint cannot be generally fulfilled. Hence the one-dimensional wave considerations must allow for a jump in the normal component of the **B**-field.

In the method developed by Powell and others [1, 12, 36, 38] the derivation of one-dimensional fluxes is based on the symmetrizable form of the MHD equations, which was introduced by Godunov [25]. In the original approach, a Roe-type solver for a modified system is used which admits jumps in the normal component of the magnetic field and advects them with the fluid velocity. Additionally, some "source terms" which are proportional to $\nabla \cdot \mathbf{B}$ are evaluated in each time step. It was discovered later that the robustness of a MHD code can be improved just by adding these so-called divergence source terms to an arbitrary solver [44].

For the time-dependent Maxwell equations, Assous *et al.* [3] introduced a Lagrange multiplier to couple the divergence constraints with the hyperbolic evolution equations for the electric and magnetic field. This enlarged system is then solved using a finite-element method in which the divergence condition is enforced via a penalization technique. For finite-element methods the least-squares approach also turned out to be a good candidate for approximately satisfying the evolution equations together with the divergence constraints [27, 28, 40, 42]. One can apply an operator-splitting procedure to the Lagrange multiplier formulation: In the first step the hyperbolic evolution equations are solved numerically; in the second step the elliptic divergence constraint is enforced by solving an elliptic equation for the Lagrange multiplier. Thus the formulation by Assous *et al.* [3] is reduced to the projection method for the Maxwell equations proposed by Boris [10]. Munz *et al.* [34, 35] modified the Lagrange multiplier formulation and called this system the generalized Lagrange multiplier (GLM) formulation of the Maxwell equations. The equation for the generalized Lagrange multiplier may be chosen to be elliptic, parabolic, or hyperbolic. In the first case the projection method and in the second case the parabolic approach of Marder [32] is rediscovered. The hyperbolic approach seems to be an attractive divergence cleaning method, especially within the framework of finite-volume schemes. The GLM–Maxwell equations become purely hyperbolic in this case; the divergence errors are transported to the boundary by waves with finite speed. For all three choices it has been shown that the divergence errors are bounded in time if charge conservation is not exactly satisfied, which does not hold for the unmodified Maxwell system (see [35]).

The outline of this paper is as follows: In Section 2 we introduce and discuss constrained formulations of the MHD equations. The eigensystem of the GLM–MHD equations is investigated in Section 3. Our implementation of the purely hyperbolic and mixed hyperbolic/parabolic approaches is described in Section 4. The resulting algorithm permits the use of any existing MHD solver *without modifications* on arbitrary grids and is local in space and time. Numerical examples are considered in Section 5. We compare the results of our new

approach with calculations obtained using the Powell source terms or without using any divergence correction. We do not consider other techniques, such as the Hodge projection or staggered grids, since we want to focus on methods which can be used as simple add-ons to existing finite-volume codes on arbitrary grids and do not require nonlocal operations or other fundamental changes in the implementation. For a comparison of the source term approach, the projection scheme, and constrained transport/central difference type schemes on structured grids we refer to [43]. Finally, our conclusions are given in Section 6. Analytical results concerning the behavior of divergence errors in the one-dimensional case are discussed in the Appendix.

2. CONSTRAINED FORMULATIONS OF THE MHD EQUATIONS

In [34, 35] the divergence constraint for the electric field **E** in the Maxwell equations has been coupled with the evolution equation for **E** by introducing a new unknown function ψ. Different possibilities for this correction have been examined, which lead to an elliptic, a parabolic, or a hyperbolic equation for ψ. We suggest using the same approach to couple the divergence constraint (2) for the magnetic field **B** with the hyperbolic evolution equations (1a)–(1d). Equation (2) and the equations for the magnetic induction (1c) are thus replaced by

$$\partial_t \mathbf{B} + \nabla \cdot (\mathbf{u}\mathbf{B}^T - \mathbf{B}\mathbf{u}^T) + \nabla\psi = 0, \tag{4}$$

$$\mathcal{D}(\psi) + \nabla \cdot \mathbf{B} = 0, \tag{5}$$

where $\mathcal{D}$ is a linear differential operator. Hence a new unknown function ψ which couples the divergence constraint to the hyperbolic system is introduced. We try to choose $\mathcal{D}$ and the initial and boundary conditions for ψ in such a way that a numerical approximation to (4), (5) is a good approximation to the original system (1c), (2). In the following we describe different choices for the linear operator $\mathcal{D}$ according to the suggestions in [34, 35]. Theoretical justification for some of these approaches is given in the Appendix.

For sufficiently smooth solutions we obtain

$$\partial_t(\nabla \cdot \mathbf{B}) + \Delta\psi = 0, \tag{6}$$

$$\partial_t \mathcal{D}(\nabla \cdot \mathbf{B}) + \Delta\mathcal{D}(\psi) = 0, \tag{7}$$

$$\partial_t \mathcal{D}(\psi) + \partial_t(\nabla \cdot \mathbf{B}) = 0, \tag{8}$$

$$\Delta\mathcal{D}(\psi) + \Delta(\nabla \cdot \mathbf{B}) = 0 \tag{9}$$

from (4) and (5), respectively. Thus we have

$$\partial_t \mathcal{D}(\nabla \cdot \mathbf{B}) - \Delta(\nabla \cdot \mathbf{B}) = 0, \tag{10}$$

$$\partial_t \mathcal{D}(\psi) - \Delta\psi = 0; \tag{11}$$

i.e., $\nabla \cdot \mathbf{B}$ and ψ satisfy the same equation for any choice of $\mathcal{D}$.

If we choose

$$\mathcal{D}(\psi) := 0, \tag{12}$$

then ψ is just a Lagrange multiplier. Within the numerical framework we can apply the following two-step method in the spirit of an operator-splitting approach: In the first step

the hyperbolic system (1a)–(1d) is solved, resulting in a magnetic field $\mathbf{B}^{n^*}$. For ψ we discretize Eq. (6) with respect to time,

$$-\Delta\psi^{n^*} = \frac{1}{\Delta t_n}(\nabla\cdot\mathbf{B}^{n^*} - \nabla\cdot\mathbf{B}^n) = \frac{1}{\Delta t_n}\nabla\cdot\mathbf{B}^{n^*}.$$

For the last equality we have assumed that the magnetic field at time t^n is divergence-free. In the second step the magnetic field is updated by solving an approximation of the equation $\partial_t\mathbf{B} = -\nabla\psi$,

$$\mathbf{B}^{n+1} = \mathbf{B}^{n^*} - \Delta t_n\nabla\psi^{n^*}.$$

Hence $\mathbf{B}^{n+1}$ is simply the projection of $\mathbf{B}^{n^*}$ into the space of divergence-free vector fields, as introduced by Brackbill and Barnes [12]. We call this approach *elliptic* correction, since a Poisson equation is solved for the function ψ.

A *parabolic* correction is obtained by defining

$$\mathcal{D}(\psi) := \frac{1}{c_p^2}\psi \quad \text{with } c_p \in (0,\infty), \tag{13}$$

since (11) turns out to be the heat equation

$$\partial_t\psi - c_p^2\Delta\psi = 0. \tag{14}$$

Thus the local divergence errors are dissipated and smoothed out if suitable boundary conditions are used (see also the Appendix). Note that in the parabolic case no additional scalar field is required since ψ can be eliminated from (4): Substituting (13) into (5) leads to a trivial equation for ψ. If its solution is substituted into (4) we obtain the equation

$$\partial_t\mathbf{B} + \nabla\cdot(\mathbf{u}\mathbf{B}^T - \mathbf{B}\mathbf{u}^T) = c_p^2\nabla(\nabla\cdot\mathbf{B}),$$

where the right-hand side can be rewritten in divergence form.

The most interesting choice for the construction of finite-volume schemes is the *hyperbolic* correction where

$$\mathcal{D}(\psi) := \frac{1}{c_h^2}\partial_t\psi \quad \text{with } c_h \in (0,\infty). \tag{15}$$

In this case, (11) is the wave equation

$$\partial_{tt}^2\psi - c_h^2\Delta\psi = 0; \tag{16}$$

local divergence errors are propagated to the boundary with the finite speed $c_h > 0$ (see also the Appendix). Moreover, the system (1a), (1b), (4), (1d), (5) is purely hyperbolic.

We want to obtain a fully explicit approximation to the MHD equations which is local with respect to space. Therefore, we use neither the elliptic correction nor an implicit approximation of the parabolic correction.

In [33] a simplified model for the MHD divergence problem is investigated. It turns out that an explicit scheme for the parabolic approach gives rather unsatisfying results

due to the stability conditions restricting the choice of c_p. (Preliminary tests for the full MHD system point in the same direction. In addition, the implementation of the parabolic approach on unstructured grids is not straightforward.) This difficulty is overcome by using a combination of the parabolic and the hyperbolic ansatz; the results obtained in [33] for this choice are very encouraging. To adapt this *mixed* correction to our situation we have to use

$$\mathcal{D}(\psi) := \frac{1}{c_h^2}\partial_t\psi + \frac{1}{c_p^2}\psi. \tag{17}$$

Now Eq. (11) is equal to the telegraph equation [23]

$$\partial_{tt}^2\psi + \frac{c_h^2}{c_p^2}\partial_t\psi - c_h^2\Delta\psi = 0 \tag{18}$$

and offers both dissipation and propagation of divergence errors. The "divergence constraint" (5) takes the form

$$\partial_t\psi + c_h^2\nabla\cdot\mathbf{B} = -\frac{c_h^2}{c_p^2}\psi. \tag{19}$$

Since the damping is now achieved by a source term instead of an explicit dissipation, there is no longer a restriction on c_p imposed by a stability condition. Note that the only source term occurs in the equation for the unphysical variable ψ. The mixed correction can be formally reduced to the hyperbolic correction if we set $c_p := \infty$.

As proposed in [34, 35] for the Maxwell equations, the system (1a), (1b), (4), (1d), (5) is called the generalized Lagrange multiplier (GLM) formulation of the MHD equations. It is worth noting that for the hyperbolic and mixed corrections considered above, the GLM–MHD system is hyperbolic and the variables ρ, $\rho\mathbf{u}$, $\mathbf{B}$, and e are still conserved (see also Section 3).

A slightly different constrained formulation is obtained if we derive the MHD equations from the GLM–Maxwell equations instead of correcting the MHD equations directly. Assuming that the time evolution of the electric field can be neglected, the GLM–Maxwell equations from [34, 35] with corrections affecting $\nabla\cdot\mathbf{B}$ read

$$\nabla\times\mathbf{B} = \mathbf{j}, \tag{20a}$$

$$\partial_t\mathbf{B} + \nabla\times\mathbf{E} + \nabla\psi = 0, \tag{20b}$$

$$\mathcal{D}(\psi) + \nabla\cdot\mathbf{B} = 0. \tag{20c}$$

Here $\mathbf{E}$ denotes the electric field and $\mathbf{j}$ the current density. As before, the coupling of the time evolution equation (20b) and the divergence condition (20c) is achieved by the function ψ and the linear differential operator $\mathcal{D}$.

Instead of combining the usual Maxwell equations with the fluid equations, we take the modified equations (20a)–(20c). In the fluid equations the influence of the magnetic field appears as an external force: The Lorentz force

$$\mathbf{F}_L := \mathbf{j}\times\mathbf{B} \tag{21}$$

completes the momentum equations, while $\mathbf{F}_L \cdot \mathbf{u}$ supplements the energy equation. Equation (20a) and some simple calculations yield the identities

$$\mathbf{F}_L = (\nabla \times \mathbf{B}) \times \mathbf{B} = \nabla \cdot \left(\mathbf{B}\mathbf{B}^T - \frac{1}{2}\mathbf{B}^2 \mathcal{I} \right) - (\nabla \cdot \mathbf{B})\mathbf{B}. \tag{22}$$

In the momentum equation the part in divergence form is added to the flux, while the second term is considered to be a "source term." Usually this second term is dropped, assuming that the magnetic field is divergence-free. The total energy e consists of the hydrodynamic energy and the magnetic energy $|\mathbf{B}|^2/2$. By means of considerations similar to those in (22) we obtain the source term $-\mathbf{B} \cdot (\nabla \psi)$ for the energy equation. Furthermore, in the magnetohydrodynamic case Ohm's law reads

$$\mathbf{E} = -\mathbf{u} \times \mathbf{B}. \tag{23}$$

Using (23) we derive the magnetic field equations from (20b). The resulting system reads

$$\partial_t \rho + \nabla \cdot (\rho \mathbf{u}) = 0, \tag{24a}$$

$$\partial_t (\rho \mathbf{u}) + \nabla \cdot \left[\rho \mathbf{u}\mathbf{u}^T + \left(p + \frac{1}{2}\mathbf{B}^2 \right) \mathcal{I} - \mathbf{B}\mathbf{B}^T \right] = -(\nabla \cdot \mathbf{B})\mathbf{B}, \tag{24b}$$

$$\partial_t \mathbf{B} + \nabla \cdot (\mathbf{u}\mathbf{B}^T - \mathbf{B}\mathbf{u}^T + \psi \mathcal{I}) = 0, \tag{24c}$$

$$\partial_t e + \nabla \cdot \left[\left(e + p + \frac{1}{2}\mathbf{B}^2 \right) \mathbf{u} - \mathbf{B}(\mathbf{u} \cdot \mathbf{B}) \right] = -\mathbf{B} \cdot (\nabla \psi), \tag{24d}$$

$$\partial_t \psi + c_h^2 \nabla \cdot \mathbf{B} = -\frac{c_h^2}{c_p^2} \psi. \tag{24e}$$

Since it equals the GLM–MHD system (1a), (1b), (4), (1d), (5) *extended* by additional terms on the right-hand side, we call this approach the extended GLM (EGLM) formulation of the MHD equations.

3. EIGENSYSTEM OF THE CONSTRAINED MHD EQUATIONS

In this section we study the eigensystem of the GLM– and EGLM–MHD systems. We compare its structure with that obtained for the original MHD equations and for the system with divergence source terms [25, 36]. Furthermore, we show how the GLM– and EGLM–MHD system can be modified to achieve Galilean invariance.

First we consider the GLM–MHD equations (1a), (1b), (4), (1d), (5) with the mixed correction (17) in one space dimension:

$$\begin{aligned}
\partial_t \rho + \partial_x (\rho u_x) &= 0, \\
\partial_t (\rho u_x) + \partial_x \left(\rho u_x^2 + p + \frac{1}{2}\left(B_y^2 + B_z^2 - B_x^2 \right) \right) &= 0, \\
\partial_t (\rho u_y) + \partial_x (\rho u_x u_y - B_x B_y) &= 0, \\
\partial_t (\rho u_z) + \partial_x (\rho u_x u_z - B_x B_z) &= 0, \\
\partial_t B_x + \partial_x \psi &= 0,
\end{aligned} \tag{25}$$

$$\partial_t B_y + \partial_x (B_y u_x - B_x u_y) = 0,$$
$$\partial_t B_z + \partial_x (B_z u_x - B_x u_z) = 0,$$
$$\partial_t e + \partial_x \left[u_x \left(e + p + \frac{1}{2}\mathbf{B}^2 \right) - B_x (u_x B_x + u_y B_y + u_z B_z) \right] = 0,$$
$$\partial_t \psi + c_h^2 \partial_x B_x = -\frac{c_h^2}{c_p^2}\psi.$$

This system is hyperbolic, with an inhomogeneous part consisting of the source term in the last equation. To prove its hyperbolicity it suffices to show that the matrix $\mathcal{A}$ entering into the homogeneous quasi-linear form of (25),

$$\partial_t \mathbf{W} + \mathcal{A}(\mathbf{W}) \partial_x \mathbf{W} = 0, \tag{26}$$

is diagonalizable with real eigenvalues. Here $\mathbf{W} = (\rho, u_x, u_y, u_z, B_x, B_y, B_z, p, \psi)^T$ is the vector of primitive variables and we find

$$\mathcal{A}(\mathbf{W}) = \begin{pmatrix} u_x & \rho & 0 & 0 & 0 & 0 & 0 & 0 & 0 \\ 0 & u_x & 0 & 0 & -\frac{B_x}{\rho} & \frac{B_y}{\rho} & \frac{B_z}{\rho} & \frac{1}{\rho} & 0 \\ 0 & 0 & u_x & 0 & -\frac{B_y}{\rho} & -\frac{B_x}{\rho} & 0 & 0 & 0 \\ 0 & 0 & 0 & u_x & -\frac{B_z}{\rho} & 0 & -\frac{B_x}{\rho} & 0 & 0 \\ 0 & 0 & 0 & 0 & 0 & 0 & 0 & 0 & 1 \\ 0 & B_y & -B_x & 0 & -u_y & u_x & 0 & 0 & 0 \\ 0 & B_z & 0 & -B_x & -u_z & 0 & u_x & 0 & 0 \\ 0 & \gamma p & 0 & 0 & (\gamma - 1)\mathbf{u} \cdot \mathbf{B} & 0 & 0 & u_x & (1-\gamma) B_x \\ 0 & 0 & 0 & 0 & c_h^2 & 0 & 0 & 0 & 0 \end{pmatrix}. \tag{27}$$

From the structure of $\mathcal{A}$ we see again that the equations for B_x and ψ are decoupled from the remaining system. If we define $\mathbf{W}' := (\rho, u_x, u_y, u_z, B_y, B_z, p)^T$ and if $\mathcal{A}'(\mathbf{W}')$ is obtained from $\mathcal{A}(\mathbf{W})$ by cancelling the fifth and ninth row and column, then

$$\partial_t \mathbf{W}' + \mathcal{A}'(\mathbf{W}') \partial_x \mathbf{W}' = 0 \tag{28}$$

is the usual one-dimensional MHD system in primitive variables which is obtained using (2). In this case we regard B_x as a parameter. $\mathcal{A}'$ has seven linearly independent right eigenvectors (see, e.g., [47]) and is therefore diagonalizable. Its eigenvalues are u_x, $u_x \pm c_s$, $u_x \pm c_a$, $u_x \pm c_f$. The speeds $c_s \le c_a \le c_f$ are given by

$$c_a = |b_x|, \tag{29}$$
$$c_f = \sqrt{\frac{1}{2}\left(a^2 + b^2 + \sqrt{(a^2+b^2)^2 - 4a^2 b_x^2}\right)}, \tag{30}$$
$$c_s = \sqrt{\frac{1}{2}\left(a^2 + b^2 - \sqrt{(a^2+b^2)^2 - 4a^2 b_x^2}\right)} \tag{31}$$

using the abbreviations

$$b_x := \sqrt{\frac{B_x^2}{\rho}}, \quad b^2 := \frac{|\mathbf{B}|^2}{\rho}, \quad a := \sqrt{\frac{\gamma p}{\rho}}. \tag{32}$$

For any right eigenvector $\mathbf{r}' = (r_1', \dots, r_7')^T$ of $\mathcal{A}'$ we obtain a right eigenvector $\mathbf{r}$ of $\mathcal{A}$ by choosing $\mathbf{r} := (r_1', \dots, r_4', 0, r_5', \dots, r_7', 0)^T$ with respect to the same eigenvalue. Moreover, due to the decoupling of the fifth and ninth equation in (25) $\mathcal{A}$ has the additional eigenvalues $-c_h$ and c_h. These are distinct from the eigenvalues of $\mathcal{A}'$ if c_h is sufficiently large. Hence $\mathcal{A}$ has nine linearly independent right eigenvectors and its eigenvalues read in nondecreasing order

$$\lambda_1 = -c_h, \quad \lambda_2 = u_x - c_f, \quad \lambda_3 = u_x - c_a, \quad \lambda_4 = u_x - c_s, \quad \lambda_5 = u_x,$$
$$\lambda_6 = u_x + c_s, \quad \lambda_7 = u_x + c_a, \quad \lambda_8 = u_x + c_f, \quad \lambda_9 = c_h.$$

Thus we have shown that the system (25) is hyperbolic. Furthermore, the structure of the right eigenvectors shows that only the waves traveling with speeds λ_1 and λ_9 can carry a change in B_x or ψ. We note that these two additional waves extend the idea of a divergence wave introduced by Powell and others [1, 12, 36, 38].

In the following we want to study the behavior of the EGLM system (24a)–(24e) in the mixed case (17) and of the MHD system (1a)–(1d) with the "divergence source terms" (36) in one space dimension. If we omit the source term in (24e), as in the GLM case considered above, both systems can be written in the form

$$\partial_t \mathbf{U} + \partial_x \mathbf{F}(\mathbf{U}) = \mathcal{S}(\mathbf{U}) \partial_x \mathbf{U}, \tag{33}$$

where $\mathbf{U} := (\rho, \rho u_x, \rho u_y, \rho u_z, B_x, B_y, B_z, e, \psi)^T$ are the conservative variables, $\mathbf{F}$ is the flux vector in x-direction, and $\mathcal{S}(\mathbf{U}) \in \mathbb{R}^{9\times 9}$. For sufficiently smooth solutions (33) is equivalent to

$$\partial_t \mathbf{W} + (\mathcal{A}(\mathbf{W}) - \mathcal{B}(\mathbf{W})) \partial_x \mathbf{W} = 0, \tag{34}$$

with $\mathcal{B}(\mathbf{W}) := \frac{\partial \mathbf{W}}{\partial \mathbf{U}} \mathcal{S}(\mathbf{U}(\mathbf{W})) \frac{\partial \mathbf{U}}{\partial \mathbf{W}}$. (Note that $\mathcal{A}(\mathbf{W}) = \frac{\partial \mathbf{W}}{\partial \mathbf{U}} D\mathbf{F}(\mathbf{U}) \frac{\partial \mathbf{U}}{\partial \mathbf{W}}$ if $D\mathbf{F}(\mathbf{U})$ denotes the Jacobian of $\mathbf{F}(\mathbf{U})$.)

If we consider the EGLM system (24a)–(24e), we obtain

$$\mathcal{B}_{EGLM}(\mathbf{W}) = \begin{pmatrix} 0 & 0 & 0 & 0 & 0 & 0 & 0 & 0 & 0 \\ 0 & 0 & 0 & 0 & -\frac{B_x}{\rho} & 0 & 0 & 0 & 0 \\ 0 & 0 & 0 & 0 & -\frac{B_y}{\rho} & 0 & 0 & 0 & 0 \\ 0 & 0 & 0 & 0 & -\frac{B_z}{\rho} & 0 & 0 & 0 & 0 \\ 0 & 0 & 0 & 0 & 0 & 0 & 0 & 0 & 0 \\ 0 & 0 & 0 & 0 & 0 & 0 & 0 & 0 & 0 \\ 0 & 0 & 0 & 0 & 0 & 0 & 0 & 0 & 0 \\ 0 & 0 & 0 & 0 & 0 & 0 & 0 & 0 & (1-\gamma)B_x \\ 0 & 0 & 0 & 0 & 0 & 0 & 0 & 0 & 0 \end{pmatrix}. \tag{35}$$

It is obvious that $\mathcal{A} - \mathcal{B}_{EGLM}$ has the same eigenvalues $\lambda_1, \ldots, \lambda_9$ and right eigenvectors $\mathbf{r}_2, \ldots, \mathbf{r}_8$ as $\mathcal{A}$ itself. One disadvantage of the EGLM approach is that we have nonconservative hyperbolic terms on the right-hand side of (24a)–(24e). Thus in the numerical approximation rounding errors and discretization errors may lead to a violation of conservation, even if the initial values are divergence-free. Possible consequences of a lack of conservation are discussed in Section 5.

For divergence-free initial conditions the MHD equations (1a)–(1d) can only be symmetrized if some hyperbolic terms are added on the right-hand side [8, 25]:

$$\begin{aligned}
\partial_t \rho + \nabla \cdot (\rho \mathbf{u}) &= 0, \\
\partial_t (\rho \mathbf{u}) + \nabla \cdot \left[\rho \mathbf{u}\mathbf{u}^T + \left(p + \frac{1}{2}\mathbf{B}^2 \right) \mathcal{I} - \mathbf{B}\mathbf{B}^T \right] &= -(\nabla \cdot \mathbf{B})\mathbf{B}, \\
\partial_t \mathbf{B} + \nabla \cdot (\mathbf{u}\mathbf{B}^T - \mathbf{B}\mathbf{u}^T) &= -(\nabla \cdot \mathbf{B})\mathbf{u}, \\
\partial_t e + \nabla \cdot \left[\left(e + p + \frac{1}{2}\mathbf{B}^2 \right) \mathbf{u} - \mathbf{B}(\mathbf{u} \cdot \mathbf{B}) \right] &= -(\nabla \cdot \mathbf{B})\mathbf{u} \cdot \mathbf{B}.
\end{aligned} \tag{36}$$

Numerical schemes can be stabilized against problems arising from divergence errors if they are based on (36) instead of (1a)–(1d) [1, 12, 36, 38]. The most common choice is to add a discrete version of the right-hand side of (36)—the so-called divergence source terms—to an existing solver for (1a)–(1d), (see, e.g., [44]). Since we have no equation for ψ, we formally obtain a primitive formulation of (36) if we cancel the last lines (and columns) of $\mathbf{W}$, $\mathcal{A}$, and $\mathcal{B}$ in (34); for $\mathcal{B}$ we get (cf. [36])

$$\mathcal{B}_S(\mathbf{W}) = \begin{pmatrix}
0 & 0 & 0 & 0 & 0 & 0 & 0 & 0 & 0 \\
0 & 0 & 0 & 0 & -\frac{B_x}{\rho} & 0 & 0 & 0 & 0 \\
0 & 0 & 0 & 0 & -\frac{B_y}{\rho} & 0 & 0 & 0 & 0 \\
0 & 0 & 0 & 0 & -\frac{B_z}{\rho} & 0 & 0 & 0 & 0 \\
0 & 0 & 0 & 0 & -u_x & 0 & 0 & 0 & 0 \\
0 & 0 & 0 & 0 & -u_y & 0 & 0 & 0 & 0 \\
0 & 0 & 0 & 0 & -u_z & 0 & 0 & 0 & 0 \\
0 & 0 & 0 & 0 & (\gamma - 1)\mathbf{u} \cdot \mathbf{B} & 0 & 0 & 0 & 0 \\
0 & 0 & 0 & 0 & 0 & 0 & 0 & 0 & 0
\end{pmatrix}. \tag{37}$$

Hence the fifth row of the matrix $\mathcal{A} - \mathcal{B}_S$ with last row and column canceled reads $(0, 0, 0, 0, u_x, 0, 0, 0)^T$ and as before we obtain right eigenvectors by extending those of $\mathcal{A}'$. In addition to the usual MHD eigenvalues we have an additional eigenvalue u_x with the corresponding unit vector as right eigenvector. Thus the divergence errors are transported to the boundary with the flow velocity. Again, the right-hand side of (36) causes the loss of conservation if $\nabla \cdot \mathbf{B}$ is not exactly zero.

One advantage of system (36) is its Galilean invariance. This property can easily be seen from the structure of the (reduced) matrix $\mathcal{A} - \mathcal{B}_S$: The entries on the main diagonal are all equal to u_x, and they are the only ones depending on u_x. It is easy to prove that all systems with matrices of this form are Galilean invariant. With this in mind, it is straightforward to add some hyperbolic terms to the EGLM system (24a)–(24e) (and similarly to the GLM

system (1a), (1b), (4), (1d), (5)) such that we achieve Galilean invariance:

$$\begin{aligned}
\partial_t \rho + \nabla \cdot (\rho \mathbf{u}) &= 0, \\
\partial_t (\rho \mathbf{u}) + \nabla \cdot \left[\rho \mathbf{u}\mathbf{u}^T + \left(p + \frac{1}{2}\mathbf{B}^2 \right) \mathcal{I} - \mathbf{B}\mathbf{B}^T \right] &= -(\nabla \cdot \mathbf{B})\mathbf{B}, \\
\partial_t \mathbf{B} + \nabla \cdot (\mathbf{u}\mathbf{B}^T - \mathbf{B}\mathbf{u}^T + \psi \mathcal{I}) &= -(\nabla \cdot \mathbf{B})\mathbf{u}, \\
\partial_t e + \nabla \cdot \left[\left(e + p + \frac{1}{2}\mathbf{B}^2 \right) \mathbf{u} - \mathbf{B}(\mathbf{u} \cdot \mathbf{B}) \right] &= -(\nabla \cdot \mathbf{B})\mathbf{u} \cdot \mathbf{B} - \mathbf{B} \cdot (\nabla \psi), \\
\partial_t \psi + c_h^2 \nabla \cdot \mathbf{B} &= -\mathbf{u} \cdot (\nabla \psi) - \frac{c_h^2}{c_p^2} \psi.
\end{aligned} \tag{38}$$

By doing this, we get u_x instead of 0 in the fifth and the ninth diagonal entry of $\mathcal{A} - \mathcal{B}$. Moreover, the right eigenvectors $\mathbf{r}_2, \ldots, \mathbf{r}_8$ remain valid, while λ_1 and λ_9 are changed to $u_x \mp c_h$, respectively. With this modification the GLM–MHD system is no longer conservative.

4. NUMERICAL APPROXIMATION

As noted in the introduction, our divergence cleaning technique can be easily added to any existing solver for the MHD equations. We describe this approach in the case of a first-order finite-volume scheme. However, its extension to higher order finite-volume schemes or its use together with other solvers is straightforward.

In our 2D implementation we use unstructured triangular grids, as in Fig. 1, since they allow local grid refinement without hanging nodes. For simplicity we describe the algorithm only for this setting. However, its formulation for arbitrary control volumes in 2D or even 3D is—apart from the necessity of introducing more indices—identical. One time step of our explicit finite-volume scheme for the homogeneous part of the GLM system, which is equal to the homogeneous part of the EGLM system (24a)–(24e), reads

$$\mathbf{U}_j^{n+1} = \mathbf{U}_j^n - \frac{\Delta t_n}{|T_j|} \sum_{j=1}^{3} |S_{jl}| \mathcal{R}^{-1}(\mathbf{n}_{jl}) \mathbf{G}\big(\mathcal{R}(\mathbf{n}_{jl})\mathbf{U}_j^n, \mathcal{R}(\mathbf{n}_{jl})\mathbf{U}_{jl}^n\big). \tag{39}$$

T_j is a triangle of the triangulation $\mathbb{T} = (T_i)_{1 \le i \le N}$; $\mathbf{U}_{j/jl}^n$ and $\mathbf{U}_{j/jl}^{n+1}$ denote the volume data on $T_{j/jl}$ at time t^n and t^{n+1}, respectively. S_{jl} is the common edge of T_j and T_{jl}, while $\mathbf{n}_{jl}$

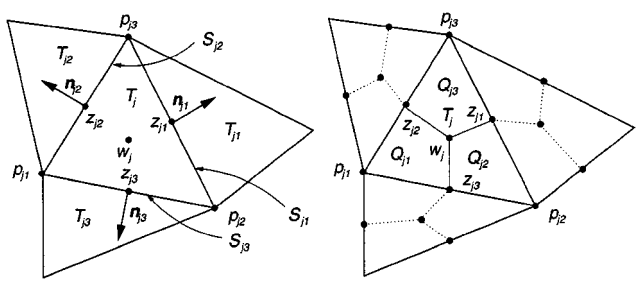

FIG. 1. Unstructured triangular grid (left) and subdivision of triangles into sections of dual cells by connecting the midpoints of the edges and the barycenters (right).

is the outer unit normal on S_{jl}. For the computation of the flux across S_{jl} we rotate T_j and T_{jl} so that $\mathbf{n}_{jl}$ is transformed into the unit vector in the x-direction. Then we evaluate $\mathbf{G}$ (denoting a numerical flux in x-direction) and rotate the triangles back. These rotations act as orthogonal mappings $\mathcal{R}(\mathbf{n}_{jl})$, $\mathcal{R}^{-1}(\mathbf{n}_{jl})$ on the data. $\Delta t_n = t^{n+1} - t^n$ is the time step, which is restricted as usual by a CFL condition: For the triangulation $\mathbb{T} = (T_i)_{1\le i\le N}$ and the constant $c_{cfl} \in (0, 1)$ we set

$$\Delta t_n := c_{cfl} \min_{1\le j\le N} \min_{1\le l\le 3} \frac{h_{jl}}{\max_{T\in\{T_j,T_{jl}\}} \left(\left| u_{\mathbf{n}_{jl}}(T) \right| + c_{f,\mathbf{n}_{jl}}(T) \right)}. \tag{40}$$

Here $h_{jl} := 2|T_j|/|S_{jl}|$ is the height of T_j in direction $\mathbf{n}_{jl}$; $u_{n_{jl}}(T)$ and $c_{f,\mathbf{n}_{jl}}(T)$ are the fluid velocity and the fast speed (cf. (30)) in T in direction $\mathbf{n}_{jl}$, respectively. The scheme (39) is (formally) extended to second order by using linear reconstruction and Runge–Kutta time integration. The indicators we use for local grid refinement and coarsening are described in [19].

In the following we first derive a numerical flux $\mathbf{G}$ for the hyperbolic GLM–MHD system. Then we describe the extension of the scheme to include the source term in the mixed GLM–MHD formulation. In a third step we turn to the EGLM–MHD system. (The source term correction is added to a scheme for the homogeneous MHD system in a similar manner.)

As we have already pointed out, the equations for B_x and ψ in (25) are decoupled from the other seven equations. In order to obtain a numerical flux $\mathbf{G}$ for the hyperbolic GLM–MHD equations, we can therefore use a numerical flux for the one-dimensional MHD equations and simply add some flux terms for the evolution equations of B_x and ψ. Hence we now construct a flux for the linear system

$$\partial_t \begin{pmatrix} B_x \\ \psi \end{pmatrix} + \begin{pmatrix} 0 & 1 \\ c_h^2 & 0 \end{pmatrix} \partial_x \begin{pmatrix} B_x \\ \psi \end{pmatrix} = \begin{pmatrix} 0 \\ 0 \end{pmatrix}. \tag{41}$$

We set the constant $c_h = c_h(t^n)$ to

$$c_h := \frac{c_{cfl}}{\Delta t_n} \min_{1\le j\le N} \min_{1\le l\le 3} h_{jl}$$

uniformly for all T_j. Thus c_h is the maximal value which is compatible with (40); that is, we have

$$\Delta t_n = c_{cfl} \min_{1\le j\le N} \min_{1\le l\le 3} \frac{h_{jl}}{c_h}.$$

The eigenvalues and corresponding right eigenvectors of (41) are $\pm c_h$ and $(1, \pm c_h)^T$, respectively. Thus it is easy to verify that the solution to the local Riemann problem with left-hand state $(B_{x,l}, \psi_l)^T$ and right-hand state $(B_{x,r}, \psi_r)^T$ has the value

$$\begin{pmatrix} B_{x,m} \\ \psi_m \end{pmatrix} = \begin{pmatrix} B_{x,l} \\ \psi_l \end{pmatrix} + \begin{pmatrix} \frac{1}{2}(B_{x,r} - B_{x,l}) - \frac{1}{2c_h}(\psi_r - \psi_l) \\ \frac{1}{2}(\psi_r - \psi_l) - \frac{c_h}{2}(B_{x,r} - B_{x,l}) \end{pmatrix} \tag{42}$$

on the cell interface. Therefore, we obtain $(\psi_m, c_h^2 B_{x,m})^T$ as numerical flux. The interface values $B_{jl}^n := B_{x,m}$ and $\psi_{jl}^n := \psi_m$ for each edge S_{jl} are stored for later use. The resulting

numerical flux $\mathbf{G}$ in (39) has the form

$$\begin{aligned}&\mathbf{G}\big(\mathcal{R}(\mathbf{n}_{jl})\mathbf{U}_j^n, \mathcal{R}(\mathbf{n}_{jl})\mathbf{U}_{jl}^n\big)\\ &\quad := \mathbf{G}_{mhd}\big(\mathcal{R}(\mathbf{n}_{jl})\mathbf{U}_j^n, \mathcal{R}(\mathbf{n}_{jl})\mathbf{U}_{jl}^n; B_{jl}^n\big) + \big(0,0,0,0,\psi_{jl}^n,0,0,0,c_h^2 B_{jl}^n\big)^T. \quad (43)\end{aligned}$$

G_{mhd} is an arbitrary numerical flux for the one-dimensional MHD equations with an additional zero for the flux in ψ. Since the normal component of the magnetic field enters the corresponding flux function as a constant parameter, we have to fix its value B_{jl}^n on each edge. (For our approach, the choice $B_{jl}^n := B_{x,m}$ is the natural one; in the absence of a better choice, i.e., in the case of the uncorrected system or of the source term approach, we use $B_{jl}^n := \mathbf{n}_{jl} \cdot (\mathbf{B}_j^n + \mathbf{B}_{jl}^n)/2$.) Note that due to the divergence condition the flux for B in normal direction is zero. For G_{mhd} we use either the "simple" flux of Dai and Woodward (DW) [17] with the modifications described in [45] or the MHD–HLLEM flux proposed in [45].

The mixed GLM–MHD system differs from the hyperbolic GLM formulation only by a source term in the equation for ψ. An easy and unconditionally stable discretization is obtained by using an operator-splitting approach. We first solve the homogenous system by means of (39) and (43), which leads to the value $\psi_j^{n^*}$ for ψ on T_j. In a second step we solve the initial value problem

$$\partial_t \psi_j = -\frac{c_h^2}{c_p^2}\psi_j \quad (44)$$

with $\psi_j(0) = \psi_j^{n^*}$. We use the exact solution to (44) and set

$$\psi_j^{n+1} := e^{-\Delta t_n c_h^2/c_p^2}\psi_j^{n^*}. \quad (45)$$

While c_h has already been chosen for the solution of (41), c_p is still a free parameter. The simplest choice is to fix a constant value for $c_p \in (0, \infty)$. However, numerical tests have shown that in this case the optimal choice of c_p significantly depends on the grid size and the scheme used. Thus we suggest two other approaches, in which c_p is a function of c_h.

The first possibility is to prescribe a constant factor in (45) (i.e., to fix a constant $c_d \in (0,1)$ for $c_d := e^{-\Delta t_n c_h^2/c_p^2}$). In this case we have

$$c_p(c_d, c_h, \Delta t_n) = \sqrt{-\Delta t_n \frac{c_h^2}{\ln(c_d)}}. \quad (46)$$

A second possible choice is to fix $c_r := c_p^2/c_h \in (0, \infty)$ which mirrors the ratio between hyperbolic and parabolic effects: In the one-dimensional case the damping of divergence errors occurs on the time scale $c_p\sqrt{t}$ (cf. (A.16)); the transport of the divergence errors to the boundary takes place on the time scale $c_h t$ (cf. (A.19)). Therefore, we can fix the proportion of decay to transport by keeping the ratio c_p^2/c_h constant. For the last choice we have found that the numerical results are quite independent of the grid resolution and the scheme used. Hence we have only included results with a fixed value of c_r in the next section. However, the advantage of our new technique is evident in all three cases.

We now discuss the modifications of the scheme described so far which are necessary to approximate the EGLM–MHD system (24a)–(24e). The EGLM–MHD system is identical to the GLM–MHD system except for some additional terms on the right-hand side of the

momentum and the energy equation. These "hyperbolic" source terms are discretized in a finite-volume spirit and we add the following terms to the update for the momentum and the energy in (39), respectively:

$$\frac{1}{|T_j|}\int_{t^n}^{t^{n+1}}\int_{T_j}(\nabla\cdot\mathbf{B})(-\mathbf{B}) \approx \frac{\Delta t_n}{|T_j|}\left(-\mathbf{B}_j^n\right)\sum_{l=1}^{3}|S_{jl}|B_{jl}^n, \tag{47}$$

$$\frac{1}{|T_j|}\int_{t^n}^{t^{n+1}}\int_{T_j}(-\mathbf{B})\cdot\nabla\psi \approx \Delta t_n\left(-\mathbf{B}_j^n\right)\cdot(\nabla\psi)_j. \tag{48}$$

For the normal magnetic field on S_{jl} we again use the middle state of the Riemann solution to (42) (i.e., $B_{jl}^n = B_{x,m}$). The constant value $(\nabla\psi)_j$ is calculated from the gradient of the linear function defined by the values ψ_{jl}^n from (42) stored on the three edges of T_j.

The structure of the right-hand side of the MHD equations with Powell's source terms (36) is very similar to the source terms of the EGLM–MHD system, which are proportional to $\nabla\cdot\mathbf{B}$. Therefore we use the same technique for their discretization. Note that in this case we have no natural choice for the normal component of the magnetic field on S_{jl}. Thus we again take the average $B_{jl}^n := \mathbf{n}_{jl}\cdot(\mathbf{B}_j^n + \mathbf{B}_{jl}^n)/2$ as for the calculation of the flux $\mathbf{G}_{mhd}$ in the uncorrected MHD scheme.

While the boundary conditions for B_x and the other magnetohydrodynamic quantities have to be chosen according to the physical setting considered, we are free to prescribe a boundary condition for ψ. One possibility is to assume that the behavior of ψ and ρ at the boundary is identical. We can also use a homogeneous Dirichlet condition since ψ should vanish identically in the optimal case of a divergence-free magnetic field. A third choice is given by nonreflecting boundary conditions: If we enforce $\psi_m = \psi_l$, we obtain from (42) the condition

$$\psi_r = \psi_l + c_h(B_{x,r} - B_{x,l}). \tag{49}$$

We have tested all three approaches on different test problems. In the next section we show only results obtained with the first technique, since it is easy to add this condition to an existing code and the results have been quite satisfactory. Moreover, even if the influence of the boundary conditions does definitely depend on the problem considered, we have found no significant dependency of the mixed GLM approach on the boundary conditions. This is probably due to the damping contained in this scheme, which seems to be sufficiently large to absorb waves which are reflected at the boundaries.

5. NUMERICAL TESTS

In order to quantify the improvement achieved by our new divergence correction approach, we have to measure the divergence of the discrete solutions. While a discretization of the divergence using central finite differences is natural and consistent on Cartesian grids, it is not at all clear which discrete operator is appropriate on arbitrary grids.

Our favorite technique relies directly on the discontinuous, piecewise constant data provided by the finite-volume scheme. Using the notation introduced in Fig. 1 and within

Section 4 with $B_{jl}^n := \mathbf{n}_{jl} \cdot (\mathbf{B}_j^n + \mathbf{B}_{jl}^n)/2$ for all schemes, we define

$$\mathrm{divB}_{\mathrm{jmp}}(T_j, t^n) := \frac{1}{|T_j|} \sum_{l=1}^{3} |S_{jl}| B_{jl}^n \quad (1 \le j \le N), \tag{50}$$

$$\max_{\mathrm{jmp}}(t^n) := \max_{1 \le j \le N} \mathrm{divB}_{\mathrm{jmp}}(T_j, t^n), \tag{51}$$

$$\mathrm{L}^1_{\mathrm{jmp}}(t^n) := \sum_{1 \le j \le N} |T_j| |\mathrm{divB}_{\mathrm{jmp}}(T_j, t^n)|. \tag{52}$$

Note that the definitions (50)–(52) can be trivially extended to arbitrary grids. If $\mathbb{T}$ consists of equal-sided triangles and if $\mathbf{B}$ is sufficiently smooth, it is easy to show that

$$(\nabla \cdot \mathbf{B})(w_j, t^n) = \mathrm{divB}_{\mathrm{jmp}}(T_j, t^n) + O(h), \tag{53}$$

where h denotes the maximal triangle diameter in $\mathbb{T}$. Equation (53) also holds on Cartesian grids, since the analogon of (50) equals the central finite difference discretization of $\nabla \cdot \mathbf{B}$. Moreover, under the same assumptions we can show the relation

$$\int_\Omega |\nabla \cdot \mathbf{B}(\cdot, t^n)| \le \mathrm{L}^1_{\mathrm{jmp}}(t^n) + O(h) \tag{54}$$

for $\Omega := \cup_{1 \le j \le N} T_j$.

Another approach to evaluating the divergence uses a continuous, piecewise linear reconstruction of the finite-volume data. Formally, we construct a dual grid by connecting the midpoints of the edges and the barycenters of the triangles as sketched in Fig. 1. To obtain the values at a point p_{jl}, we add the value of T_j weighted by $|Q_{jl}| = |T_j|/3$ for all adjacent triangles and divide the sum by the volume of the dual cell with center p_{jl}. If $\mathbf{B}_{\mathrm{lin}}^n$ denotes the reconstructions of $\mathbf{B}$ at time t^n, we have $\mathbf{B}_{\mathrm{lin}}^n \in C^0(\Omega)$ and $\mathbf{B}_{\mathrm{lin}}^n|_{T_j} \in \mathbb{P}^1(T_j)$. Thus the definition

$$\mathrm{divB}_{\mathrm{lin}}(T_j, t^n) := \nabla \cdot \left(\mathbf{B}_{\mathrm{lin}}^n \,\middle|_{\,T_j}\right) \tag{55}$$

yields a constant value on each triangle. Then we can define $\max_{\mathrm{lin}}(t^n)$ and $\mathrm{L}^1_{\mathrm{lin}}(t^n)$ analogous to (51) and (52). However, the extension of this technique to arbitrary grids is not straightforward and we are not aware of a consistency result in the sense of (53) and (54). Moreover, for most numerical examples we have found $\max_{\mathrm{jmp}}(t^n) \approx \max_{\mathrm{lin}}(t^n)$ and $\mathrm{L}^1_{\mathrm{jmp}}(t^n) \approx \mathrm{L}^1_{\mathrm{lin}}(t^n)$. Hence we have decided to disregard $\max_{\mathrm{lin}}$ and $\mathrm{L}^1_{\mathrm{lin}}$ in the following. Note that the values obtained for $\max_{\mathrm{jmp}}$ are more meaningful than those for $\mathrm{L}^1_{\mathrm{jmp}}$ since the solution should be *locally* divergence-free.

We now turn to the four problems summarized in Table I. In two problems an error in $\nabla \cdot \mathbf{B}$ is introduced either by the initial data (peak in B_x) or by the boundary conditions (shock reflection), while the initial data and boundary conditions for the 1D and 2D Riemann problem as well as for the Kelvin–Helmholtz instability are divergence-free even on the discrete level. For the problems with periodic boundary conditions we can check how strongly the conservation is affected if schemes with hyperbolic source terms are used. Furthermore we know—at least to some extent—the exact solutions for the shock reflection

TABLE I
Initial Data for 2D Test Problems

Peak in B_x ($\gamma = 5/3$)
Computational domain: $[-0.5, -0.5] \times [1.5, 1.5]$
Boundaries: periodic

ρ	u_x	u_y	u_z	B_x	B_y	B_z	p
1.0	1.0	1.0	0.0	$r(x^2+y^2)/\sqrt{4\pi}$	0.0	$1/\sqrt{4\pi}$	6.0

$r(s) := 4096\,s^4 - 128\,s^2 + 1$

1D Riemann problem ($\gamma = 5/3$)
Computational domain: $[-0.5, 0.5] \times [-0.25, 0.25]$
Boundaries: Neumann condition on left and right, periodic on top and bottom

	ρ	u_x	u_y	u_z	B_x	B_y	B_z	p
$x < 0$	1.0	10.0	0.0	0.0	$5/\sqrt{4\pi}$	$5/\sqrt{4\pi}$	0.0	20.0
$x > 0$	1.0	−10.0	0.0	0.0	$5/\sqrt{4\pi}$	$5/\sqrt{4\pi}$	0.0	1.0

Shock reflection ($\gamma = 1.4$)
Computational domain: $[-1, 1] \times [-0.5, 0.5]$
Boundaries: Dirichlet condition on top and left with constant data $\mathbf{U}_t$ and $\mathbf{U}_l$, reflecting bottom (symmetry), and Neumann conditions on the right
Initial data: $\mathbf{U}_0 = \mathbf{U}_l$

Data	ρ	u_x	u_y	u_z	B_x	B_y	B_z	p
$\mathbf{U}_l$	1.0	2.9	0.0	0.0	0.5	0.0	0.0	5/7
$\mathbf{U}_t$	1.4598	2.7170	−0.4049	0.0	0.6838	−0.1019	0.0	1.2229

2D Riemann problem ($\gamma = 5/3$)
Computational domain: $[-1, 1] \times [-1, 1]$
Boundaries: Dirichlet condition (numerical solution to 1D Riemann problems)
Quadrants: I, $x > 0, y > 0$; II, $x < 0, y > 0$; III, $x < 0, y < 0$; IV, $x > 0, y < 0$

Qdr.	ρ	ρu_x	ρu_y	ρu_z	B_x	B_y	B_z	e
I	0.9308	1.4557	−0.4633	0.0575	0.3501	0.9830	0.3050	5.0838
II	1.0304	1.5774	−1.0455	−0.1016	0.3501	0.5078	0.1576	5.7813
III	1.0000	1.7500	−1.0000	0.0000	0.5642	0.5078	0.2539	6.0000
IV	1.8887	0.2334	−1.7422	0.0733	0.5642	0.9830	0.4915	12.999

Kelvin–Helmholtz instability ($\gamma = 1.4$)
Computational domain: $[0, 1] \times [-1, 1]$
Boundaries: periodic

ρ	u_x	u_y	u_z	B_x	B_y	B_z	p
1.0	$u_x^0(x,y)$	$u_y^0(x,y)$	0.0	1.0	0.0	0.0	50.0

$u_x^0(x,y) := 5(\tanh(20(y+0.5)) - (\tanh(20(y-0.5)) + 1))$,
$u_y^0(x,y) := 0.25\sin(2\pi x)(e^{-100(y+0.5)^2} - e^{-100(y-0.5)^2})$

and the Riemann problems. For the 1D Riemann problem we used the first-order DW and MHD–HLLEM schemes. All other calculations were performed for both the second-order DW scheme and the second-order MHD–HLLEM scheme (see Section 4). For the peak in B_x and the 1D Riemann problem we used globally refined grids with different resolutions, while for the other problems the grid was locally adapted. The time step was computed according to (40) using $c_{cfl} := 0.3$. The choice of contour levels is identical throughout Fig. 3 and within each line of Figs. 5, 6, and 8. Since there are almost no visible differences

TABLE II
L^1 Error and eoc for the 1D Riemann Problem

	Mixed EGLM		Mixed GLM		Source terms	
Elements	L^1 error	eoc	L^1 error	eoc	L^1 error	eoc
1,024	6.44165126		6.45517676		7.03537990	
4,096	3.08112407	1.064	3.09306537	1.061	3.82213248	0.880
16,384	1.68278946	0.873	1.68627598	0.875	2.48360779	0.622
65,536	0.97173595	0.792	0.96600380	0.804	1.84060872	0.432
262,144	0.47211608	1.041	0.46045425	1.069	No solution	
1,048,576	0.23998602	0.976	0.22792806	1.014	No solution	

Note. The errors are computed between a 1D reference solution, with $h = 0.0002$ and 1D cuts of the 2D solutions at $y = 0.0424$.

between the mixed GLM and the mixed EGLM solutions, results obtained for the mixed EGLM approach are only included in Table II and Fig. 6.

For the peak in B_x we have found that the optimal value of c_r is about 0.18 *independent* of the grid resolution and the order of the scheme (see Fig. 2). Hence we use $c_r := 0.18$ for the mixed GLM and the mixed EGLM ansatz throughout this paper. Figure 3 shows that the impact of the different approaches on the numerical solution with 65,536 triangles is quite different: If the Powell source terms are used, the initial peak in B_x is simply advected with the flow velocity; without any correction we get new maxima and minima in the solution. Due to the faster propagation of divergence errors, the hyperbolic GLM solution shows complex wave interactions, which are not visible in the mixed GLM solution due to the additional damping. The values of $\max_{\text{jmp}}$ for the mixed GLM and mixed EGLM approaches are the smallest and almost identical; those for the hyperbolic GLM ansatz are still one order of magnitude smaller than the results with divergence sources. The worst results are obtained without divergence correction. If we also take into account the loss of conservation which occurs for the mixed EGLM and the source term approach (see Fig. 9, left), the mixed GLM ansatz is by far the best choice. Note that we obtained comparable results with the DW and MHD–HLLEM scheme for this test problem.

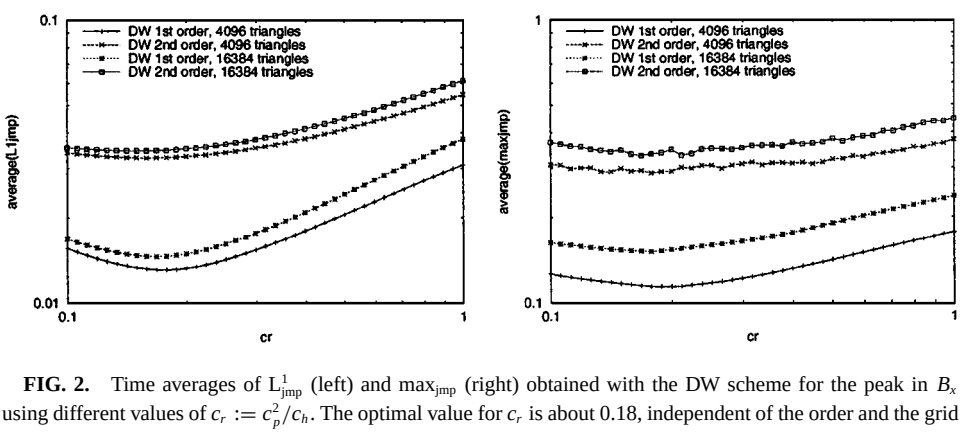

FIG. 2. Time averages of L^1_{jmp} (left) and $\max_{\text{jmp}}$ (right) obtained with the DW scheme for the peak in B_x using different values of $c_r := c_p^2/c_h$. The optimal value for c_r is about 0.18, independent of the order and the grid resolution.

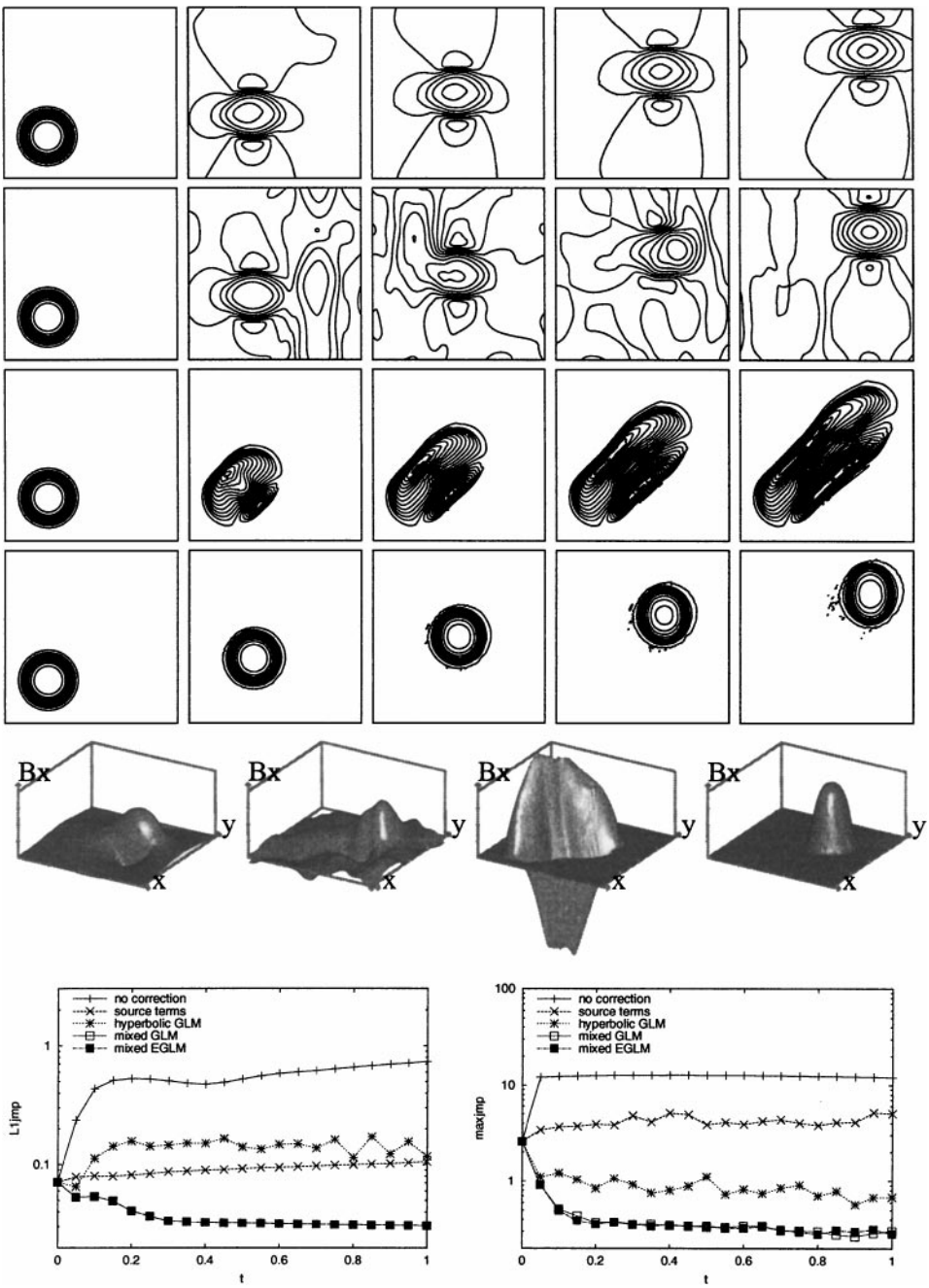

FIG. 3. Results for the peak in B_x obtained with the DW scheme on 65,536 triangles. (2D plots) Isolines of B_x at times $t = 0.0$, $t = 0.25$, $t = 0.5$, $t = 0.75$, $t = 1.0$ (from left to right) for mixed GLM and hyperbolic GLM ansatz, without correction, and with divergence source terms (from top to bottom). (3D plots) B_x at time $t = 0.75$ for mixed GLM and hyperbolic GLM ansatz, without correction, and with divergence source terms (from left to right). (1D plots) L^1_{jmp} (left) and max_{jmp} (right) for all approaches.

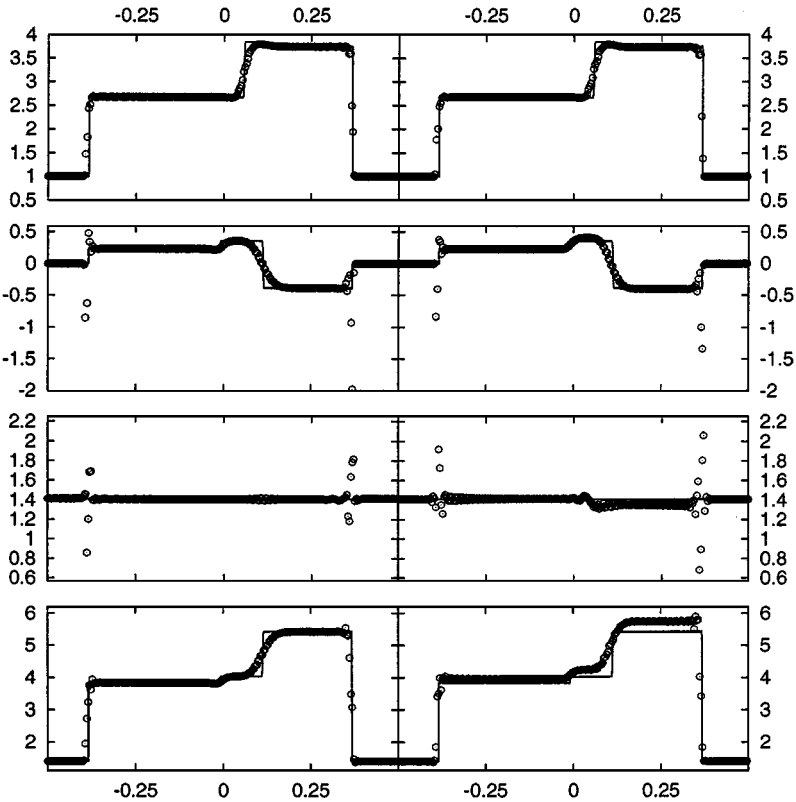

FIG. 4. Results for 1D Riemann problem obtained with the DW scheme in 2D (16,384 triangles, circles) in comparison with a 1D reference solution ($h = 0.0002$, solid line). (Left) Mixed GLM ansatz, (right) source term approach. (Top to bottom) ρ, u_y, B_x, and B_y.

By means of the 1D Riemann problem, which was originally introduced by Dai and Woodward [16] and which is also considered by Tóth [43], we want to compare the different correction approaches quantitatively. In Fig. 4 we show 1D cuts at $y = 0.0424$ of the 2D solutions obtained with the DW scheme using the mixed GLM approach and the source terms, respectively. The 1D reference solution is computed for $h = 0.0002$. In [43] it is shown that the source term approach leads to a wrong solution if this Riemann problem is solved on a rotated cartesian grid in 2D. Similarly, the source term solution on 16,384 triangles seems to contain wrong intermediate states. This observation is supported by the L^1 errors and corresponding experimental orders of convergence (eoc) given in Table II: For the mixed EGLM and the mixed GLM scheme we have a uniform first-order convergence, whereas the convergence rates decrease monotonically for the source-term approach. The divergence errors in the solutions of the source-term approach are always larger by a factor of 2 to 3 than for all of the (E)GLM methods, and for small grid sizes this method leads to negative pressure values, which results in a breakdown of the simulation. The simulations without corrections fail on all grids; the results of the hyperbolic GLM ansatz are almost identical to those of the mixed GLM approach. For the MHD–HLLEM scheme we obtain results similar to those shown in Fig. 4; in this case also the unfixed calculation succeeds and yields results comparable to those of the mixed GLM approach. However, on finer grids the simulations without corrections or with the source terms fail again.

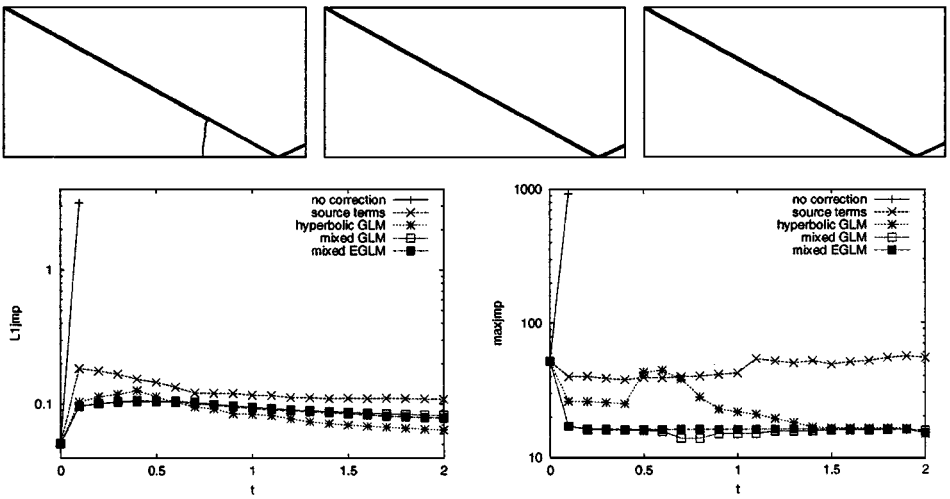

FIG. 5. Results for shock reflection obtained with the DW scheme. (Top) Isolines of ρ at time $t = 2.0$; (left to right) mixed GLM, hyperbolic GLM, and source term ansatz. (Bottom) L^1_{jmp} (left) and max_{jmp} (right).

The development of wrong intermediate states can be attributed to the lack of conservation in the source term approach. Nonconservative source terms are also involved in the mixed EGLM ansatz. Consequently, although it is not yet visible from the results shown here, a close study of the EGLM results also reveals some problems with the intermediate states, which are not present in the GLM case. However, it should be noted that we have observed clearly wrong solutions for the schemes with nonconservative source terms only for the 1D Riemann problem. In general, a violation of the divergence constraint seems to have a much stronger influence on the stability of the schemes than on the quality of the solutions. Since the problem of spurious oscillations gets more severe for smaller grid sizes, a divergence fix is especially important for simulations using locally adapted grids. We therefore study the remaining test cases on dynamically adapted grids.

The results for the shock reflection problem suggested in [2] are summarized in Fig. 5. The shock enters the domain at an angle of 29° to the x-axis; the exact solution left of the reflection point is given by the Dirichlet data on the boundaries. The difference visible in the isoline plots is due to the fact that for the mixed GLM approach the steady state is not yet fully reached. In this problem an accumulation of divergence errors causes the crash of the DW calculation without correction. The max_{jmp} errors obtained with Powell's source terms are about twice as large as the GLM and EGLM values. Moreover, after the start-up phase the L^1_{jmp} error remains constant in the simulation with source terms, while it decreases with time for the new corrections. The results for the GLM and EGLM approaches are confirmed by the MHD–HLLEM results; the only difference is that in this case the simulation with divergence source terms also breaks down as a result of divergence errors.

The initial data for the 2D Riemann problem are chosen so that the magnetic field is divergence free and the solutions of three of the four one-dimensional Riemann problems are simple waves: If we denote the quadrants by roman numbers, as in Table I, we have shocks for the problems III $\leftrightarrow$ IV and II $\leftrightarrow$ III and a rarefaction wave for I $\leftrightarrow$ II. For all five approaches the results for the density look very similar, which is not true for other components (e.g.,

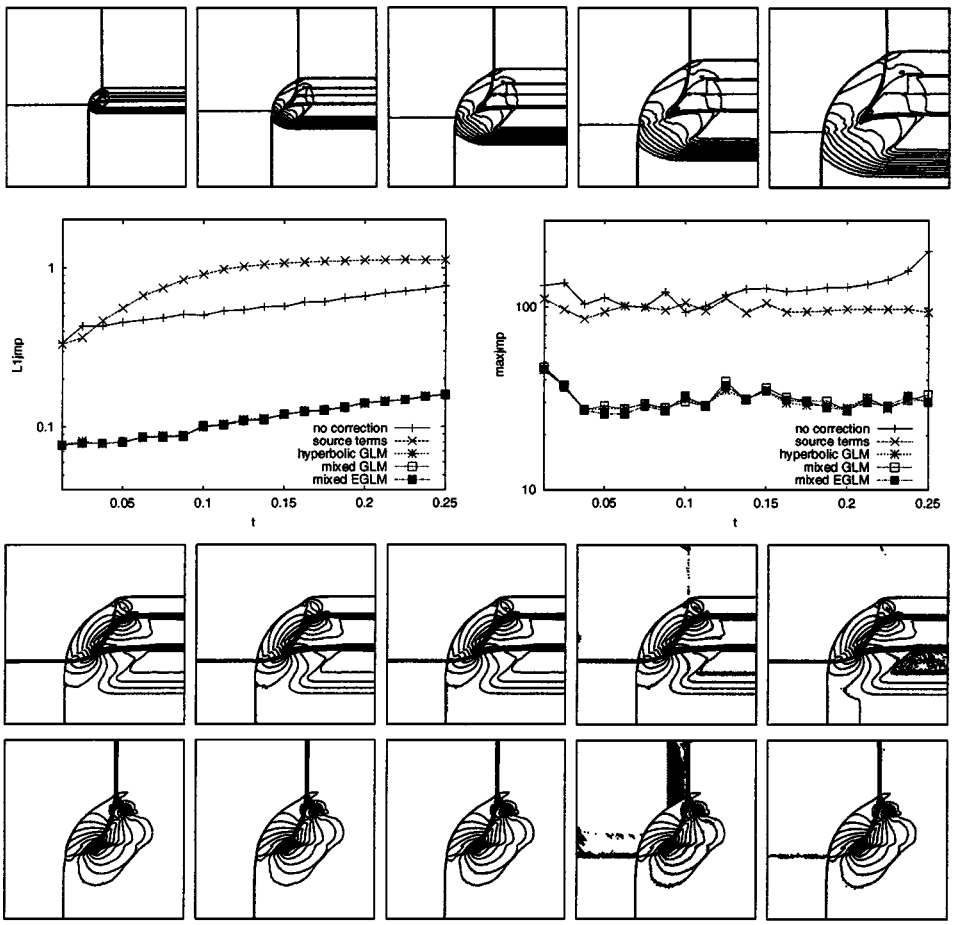

FIG. 6. Results for 2D Riemann problem obtained with the DW scheme. (Top) Isolines of ρ at times $t = 0.05$, $t = 0.1$, $t = 0.15$, $t = 0.2$ and $t = 0.25$ (from left to right) for the mixed GLM ansatz. (Middle) L^1_{jmp} (left) and max_{jmp} (right). (Bottom) Isolines of B_x (first row) and of B_y (second row) at time $t = 0.2$ for the mixed EGLM, mixed GLM, and hyperbolic GLM ansatz, without correction, and with divergence source terms (from left to right).

for the components of the magnetic field). The simulations without correction and with source terms have problems with keeping B_y constant across the shock in the II $\leftrightarrow$ III Riemann problem (see Fig. 6). Moreover, we find strong distortions in both magnetic field components behind the rarefaction wave of the I $\leftrightarrow$ II Riemann problem if no correction is used. In Fig. 7 we compare the quality of the solutions obtained for the I $\leftrightarrow$ IV Riemann problem at $x = 0.92$: For the mixed GLM ansatz the solution is very close to the 1D reference solution, while without correction we have oscillations within the rarefaction wave. For the source term approach even stronger oscillations are found right of the rarefaction wave. Note that due to the required linearization some of these high-frequency oscillations are not visible in the isoline plots of Fig. 6. The measured divergence errors for the mixed EGLM, mixed GLM, and hyperbolic GLM approaches are almost identical and at least 50% smaller than those obtained without correction or with source terms (see Fig. 6). For the distorted solutions we also observe a dramatic increase in the size of the locally adapted grids: At time $t = 0.25$ we have 166,703, 166,112, 165,194, 375,606, and 315,662 triangles for the

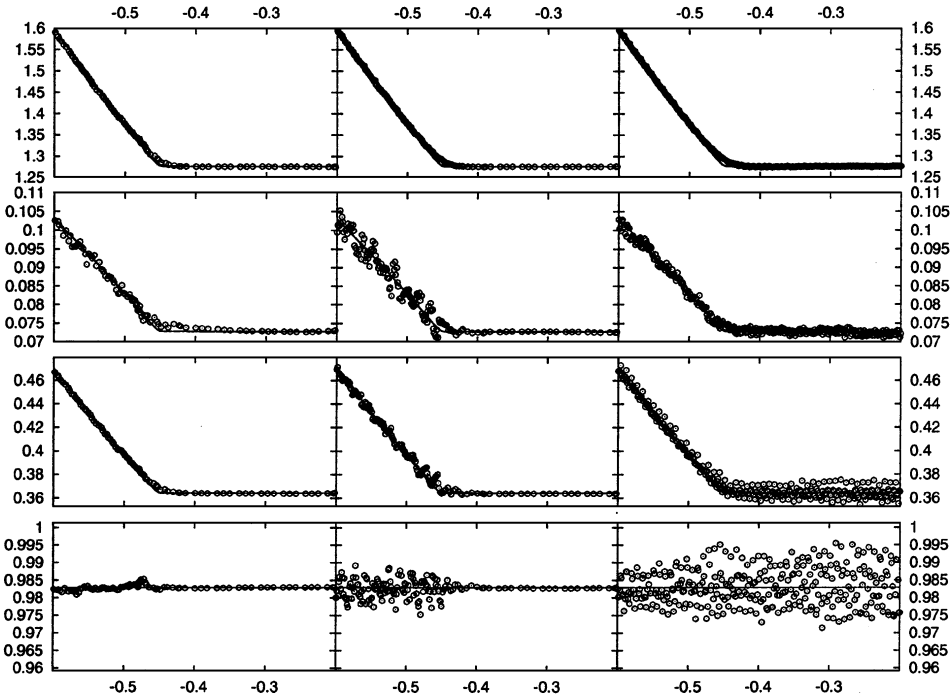

FIG. 7. Results for the 2D Riemann problem obtained with the DW scheme in 2D at $x = 0.92$ (circles) and a 1D reference solution (solid line). (Left) Mixed GLM ansatz, (middle) without correction, (right) source term approach. Displayed components (from top to bottom): u_x, B_x, and B_y; $y \in [-0.6, -0.2]$.

mixed EGLM, mixed GLM, and hyperbolic GLM ansatz, without correction, and with source terms, respectively. As a consequence, the unfixed calculation and the calculation with source terms required at least 50% more computational time than any of the (E)GLM simulations. For the MHD–HLLEM scheme we obtain results very similar to those shown in Fig. 6. The same applies to the divergence errors, even if the difference between the schemes is less striking than in the DW case. This is due to the fact that the divergence errors introduced by the MHD–HLLEM scheme itself are much smaller than those caused by the DW scheme, as was already stated in [45].

Magnetohydrodynamic Kelvin–Helmholtz instabilities have been studied in many papers (e.g., [24, 31]). Thus our last test problem illustrates the advantages our new divergence cleaning technique offers for physically relevant settings. In the isoline plots of Fig. 8 the symmetry in the DW solution with the mixed GLM approach is still well preserved, while it is quite distorted in the results obtained without correction. Moreover, the unfixed calculation required 53% more computational time—due to 12% more time steps and 36% more grid cells at the final time. As before, we see large differences in the $\max_{\text{jmp}}$ errors: For the DW scheme without correction and with Powell's source terms the errors are about the same, which is also true for the mixed GLM/EGLM approaches but on a far lower level. For the MHD–HLLEM scheme the blow-up of divergence errors causes the crash of the unfixed simulation, whereas the results of the remaining three approaches are comparable to those in the DW case. The fact that, compared to the DW scheme, the unfixed MHD–HLLEM scheme did not work as well for this problem is probably due to the better resolution of the

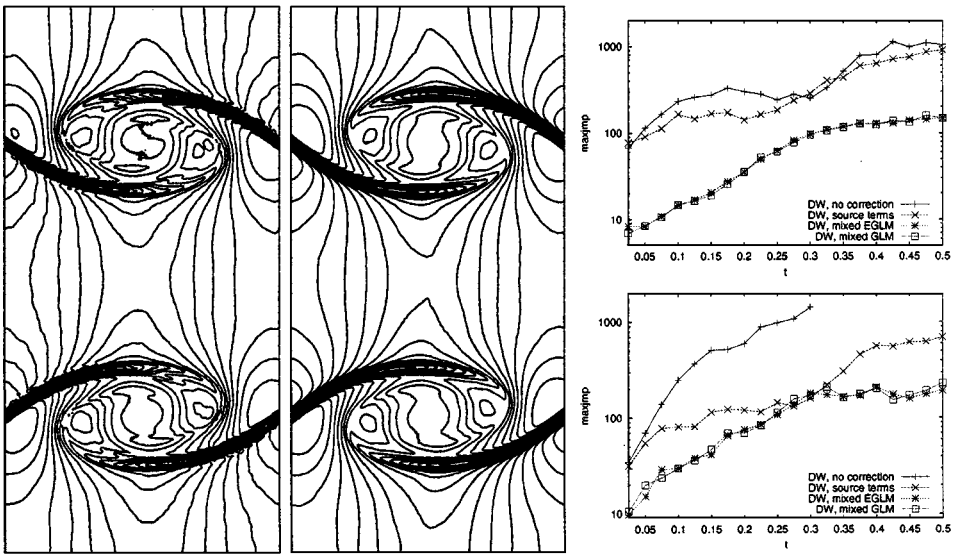

FIG. 8. Results for the Kelvin–Helmholtz instability. Isolines of ρ at time $t = 0.5$ obtained with the DW scheme without correction (left) and mixed GLM approach (middle). (Right) $\max_{\text{jmp}}$ for the DW (top) and MHD–HLLEM (bottom) schemes.

MHD–HLLEM scheme, as observed in [45], which leads to a more dynamic evolution of the solution. We remark that the plots for the L^1_{jmp} errors look similar to those for $\max_{\text{jmp}}$. The errors introduced by the hyperbolic source terms in some conservative variables are plotted in Fig. 9 (right). We see that the deviation from conservation in the source term approach is much stronger than for the mixed EGLM ansatz. Note that the discrete value of ρu_x which has to be conserved is about -10^{-9}. Hence the conservation of this quantity is a delicate task for the schemes.

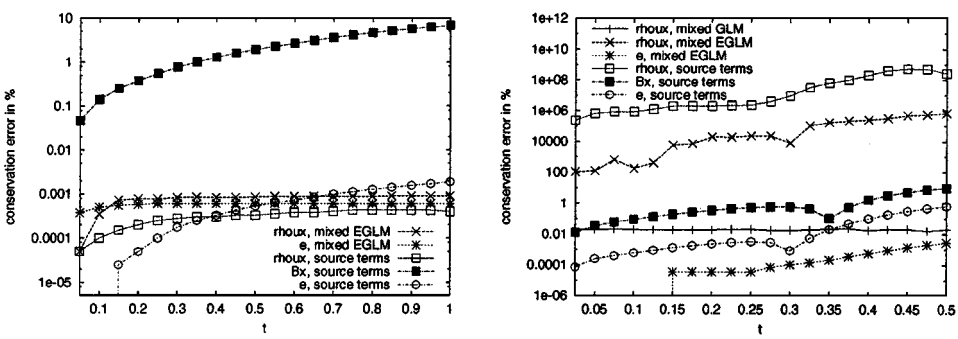

FIG. 9. Conservation errors introduced in different variables by hyperbolic source terms used with the DW scheme. (Left) Peak in B_x. (Right) Kelvin–Helmholtz instability. Without hyperbolic source terms all variables are conserved up to machine accuracy; only for ρu_x in the Kelvin–Helmholtz simulation do we observe a noticeable deviation from conservation for the mixed GLM correction (and practically the same without correction). This is due to the fact that the discrete value which has to be conserved is about -10^{-9}. Note that the relative error is increased by several orders of magnitude and keeps growing if the source terms are used.

6. CONCLUSIONS

We have derived a new divergence cleaning approach for the MHD equations by coupling the divergence constraint with the evolution equations using a generalized Lagrange multiplier (GLM). Among several possible choices, the mixed hyperbolic/parabolic GLM ansatz offers both propagation and damping of divergence errors even in stagnation points. Moreover, the magnetohydrodynamic part of the GLM–MHD system is still in conservation form. Our method is very easy to add to an existing code since the underlying MHD solver does not have to be modified. Furthermore, the only additional effort required by our method is the solution of a Riemann problem for a *linear* 2×2 system and the evaluation of a scalar source term. It is worth noting that within our new approach divergence errors are transported by two waves with speeds independent of the fluid velocity. Thus our corrections may be viewed as an extension of the "divergence wave" in the ansatz of Powell *et al.*

In our numerical tests we have found that our MHD solvers are robust and yield reliable results if we add the mixed GLM or the mixed EGLM correction. Moreover, these schemes produce smaller divergence errors than the other methods tested. We have observed a significant loss of conservation caused by hyperbolic source terms, which are not present in the mixed GLM formulation. Thus we recommend using the mixed GLM scheme.

Our method is directly applicable to ideal MHD equations on arbitrary grids in 2D and 3D. We expect that it can also be used in nonideal MHD simulations (e.g., for resistive MHD).

APPENDIX: ANALYSIS OF THE CONSTRAINED MHD EQUATIONS

In this appendix we demonstrate the effects our technique has on the evolution of a magnetic field with nonzero divergence on an analytical level. For both the parabolic and the hyperbolic GLM approach we present a theorem for the one-dimensional system which summarizes the convergence properties of the solution itself and its derivatives.

The magnetic field $\mathbf{B}$ has to satisfy

$$\partial_t \mathbf{B} + \nabla \times (\mathbf{B} \times \mathbf{u}) = 0 \quad \text{in } \mathbb{R}^3 \times \mathbb{R}^+, \tag{A.1}$$

$$\nabla \cdot \mathbf{B} = 0 \quad \text{in } \mathbb{R}^3 \times \mathbb{R}^+, \tag{A.2}$$

$$\mathbf{B}(\cdot, 0) = \mathbf{B}_0(\cdot) \quad \text{in } \mathbb{R}^3. \tag{A.3}$$

Here Eq. (A.1) is equivalent to (1c), Eq. (A.2) equals (2), and $\mathbf{B}_0$ denotes the initial data. Since $\nabla \cdot (\nabla \times \cdot) \equiv 0$ we have $\partial_t(\nabla \cdot \mathbf{B}) = 0$. This means that $\nabla \cdot \mathbf{B}(\cdot, 0) \equiv 0$ implies $\nabla \cdot \mathbf{B}(\cdot, t) \equiv 0$ for all $t > 0$. Thus the divergence constraint (A.2) is a condition for the initial data. However, in numerical simulations (A.2) can be violated. Therefore we have to study the evolution of $\mathbf{B}$ if the initial conditions have the form $\mathbf{B}(\cdot, 0) = \mathbf{B}_0(\cdot) + \mathbf{b}(\cdot)$ with $\nabla \cdot \mathbf{B}_0 = 0$ but $\nabla \cdot \mathbf{b} \neq 0$. (The disturbance $\mathbf{b}$ is due to discretization errors.) In this case the evolution equations (A.1) yield $\nabla \cdot \mathbf{B}(\cdot, t) \equiv \nabla \cdot \mathbf{b}(\cdot)$ for all $t > 0$. Hence (A.2) is not satisfied for any $t > 0$.

In one space dimension the evolution equation for $B := B_x$ in (A.1) is decoupled from the other equations. Equation (A.2) can be reduced to $\partial_x B = 0$ and the evolution equation for B reads $\partial_t B = 0$. As before, $\partial_x B(\cdot, 0) \equiv 0$ leads to $\partial_x B(\cdot, t) \equiv 0$ for all $t > 0$. Therefore B_0 (i.e., the divergence-free part of the initial data) is a constant. In order to study the evolution

of divergence errors, we have to consider the equations

$$\partial_t B = 0 \quad \text{in } \mathbb{R} \times \mathbb{R}^+, \tag{A.4}$$

$$\partial_x B = 0 \quad \text{in } \mathbb{R} \times \mathbb{R}^+, \tag{A.5}$$

$$B(\cdot, 0) = B_0 + b(\cdot) \quad \text{in } \mathbb{R} \tag{A.6}$$

with $b' \neq 0$. These equations reproduce the situation in 3D: (A.4) and (A.6) result in $B(\cdot, t) \equiv B_0 + b(\cdot)$ for all $t > 0$, which implies $\partial_x B = b' \neq 0$ independent of t. Thus (A.5) is uniformly violated. In the following we show that the situation is substantially improved if we use the GLM–MHD equations instead of the original system. If $B = B_x$ denotes the solution obtained from the one-dimensional GLM–MHD system for the initial conditions (A.6) with $b' \neq 0$, we find $|\partial_t B(x, t)| \to 0$, $|\partial_x B(x, t)| \to 0$, and $|B(x, t) - B_0| \to 0$ as $t \to \infty$. Thus for large times (A.4) and (A.5) hold at least approximately.

In the one-dimensional form of the GLM–MHD system (1a), (1b), (4), (1d), (5) the equations for B_x and ψ are decoupled from the remaining system. Therefore, we focus on the following Cauchy problem for two scalar functions $B(x, t)$, $\psi(x, t)$:

$$\partial_t B + \partial_x \psi = 0 \quad \text{in } \mathbb{R} \times \mathbb{R}^+, \tag{A.7}$$

$$\mathcal{D}(\psi) + \partial_x B = 0 \quad \text{in } \mathbb{R} \times \mathbb{R}^+, \tag{A.8}$$

$$B(\cdot, 0) = B_0 + b(\cdot) \quad \text{in } \mathbb{R}, \tag{A.9}$$

$$\psi(\cdot, 0) = \psi_0(\cdot) \quad \text{in } \mathbb{R}. \tag{A.10}$$

Here $B_0 \in \mathbb{R}$ and $b, \psi_0 \in C^2(\mathbb{R})$ are given. We investigate how different choices of $\mathcal{D}$ influence the evolution of a nonconstant $\partial_x B(\cdot, 0)$ (i.e., $b' \neq 0$). Because in practice our initial conditions are only given in a finite domain, we assume that

$$b(x) = 0 \quad \text{for } x < 0 \quad \text{and} \quad x > 1, \tag{A.11}$$

$$\psi_0(x) = 0 \quad \text{for } x < 0 \quad \text{and} \quad x > 1. \tag{A.12}$$

From Eqs. (A.7) and (A.8) we obtain (see also (10) and (11))

$$\partial_t \mathcal{D}(B) - \partial_{xx}^2 B = 0. \tag{A.13}$$

We now study the parabolic correction (13) and the hyperbolic correction (15).

THEOREM A.1: Parabolic correction. *Let $\mathcal{D}$ be given by* (13), *that is*,

$$\mathcal{D}(B) = \frac{1}{c_p^2} B \quad \text{with } c_p \in (0, \infty).$$

Then there exists a classical solution B to (A.13) *with initial conditions*

$$B(\cdot, 0) = B_0 + b(\cdot) \in C^2(\mathbb{R}). \tag{A.14}$$

The functions

$$\psi(x, t) := -c_p^2 \partial_x B(x, t) \tag{A.15}$$

and B are a solution to the system (A.7)–(A.10) *with* $\psi_0(x) = -c_p^2 b'(x)$. *Moreover, the function B fulfills the decay property*

$$|B(x,t) - B_0| \leq \|b\|_\infty \mathrm{erf}\left(\frac{1}{2c_p\sqrt{t}}\right) \quad \text{for } (x,t) \in [0,1] \times \mathbb{R}^+$$

and we have

$$\begin{aligned} |\partial_x B(x,t)| &\leq \|b'\|_\infty \mathrm{erf}\left(\frac{1}{2c_p\sqrt{t}}\right) \quad \text{for } (x,t) \in [0,1] \times \mathbb{R}^+, \\ |\partial_t B(x,t)| &\leq c_p^2 \|b''\|_\infty \mathrm{erf}\left(\frac{1}{2c_p\sqrt{t}}\right) \quad \text{for } (x,t) \in [0,1] \times \mathbb{R}^+. \end{aligned} \tag{A.16}$$

This theorem shows that the parabolic correction leads to a decay of the perturbations in the magnetic field. For large t we have approximately $B(x,t) = B_0 + O(t^{-1/2})$, so that $B(x,t) = B_0$ in the limit $t \to \infty$. Moreover, $\partial_x B$ and $\partial_t B$ also converge to zero at the same rate (i.e., (A.4) and (A.5) are satisfied for $t \to \infty$). Note that the proofs of this theorem and the following one are omitted since they completely follow standard arguments, as one can find, e.g., in [23].

We now turn to the hyperbolic correction:

THEOREM A.2: Hyperbolic correction. *Let $\mathcal{D}$ be given by* (15), *that is*,

$$\mathcal{D}(B) = \frac{1}{c_h^2}\partial_t B \quad \text{with } c_h \in (0,\infty).$$

Then there exists a classical solution B to (A.13) *with initial conditions*

$$B(\cdot,0) = B_0 + b(\cdot), \quad \partial_t B(\cdot,0) = -\psi_0'(\cdot) \quad \text{in } \mathbb{R} \tag{A.17}$$

with $b, \psi_0 \in C^2(\mathbb{R})$. The functions

$$\psi(x,t) := -c_h^2 \int_0^T \partial_x B(x,\tau)\, d\tau + \psi_0(x) \tag{A.18}$$

and B are a solution to the system (A.7)–(A.10). *Moreover, B fulfills the properties*

$$\begin{aligned} |B(x,t) - B_0| &\leq \|b\|_\infty + \frac{1}{c_h}\|\psi_0\|_\infty && \text{for } x \in [0,1] \quad \text{and} \quad 0 \leq t < \frac{1}{2c_h}, \\ |B(x,t) - B_0| &\leq \frac{1}{2}\|b\|_\infty + \frac{1}{2c_h}\|\psi_0\|_\infty && \text{for } x \in [0,1] \quad \text{and} \quad \frac{1}{2c_h} \leq t < \frac{1}{c_h}, \\ B(x,t) &= B_0 && \text{for } x \in [0,1] \quad \text{and} \quad \frac{1}{c_h} \leq t. \end{aligned}$$

Therefore it follows that

$$\partial_t B(x,t) = 0 \quad \text{and} \quad \partial_x B(x,t) = 0 \quad \text{for } x \in [0,1] \quad \text{and} \quad t \geq \frac{1}{c_h}. \tag{A.19}$$

In the case of the hyperbolic correction, we see that the perturbation is transported out of the domain $[0,1]$; after the finite time $t = \frac{1}{c_h}$ the constant value B_0 is obtained. Therefore (A.4) and (A.5) hold in $[0,1] \times (\frac{1}{c_h}, \infty)$.

ACKNOWLEDGMENTS

The authors were partially supported by the DFG priority research program "Analysis and Numerics for Conservation Laws" (ANumE) and thank Rudolf Schneider and Eric Sonnendrücker for many fruitful discussions. The comments of the reviewers were very helpful in improving this paper.

REFERENCES

1. N. Aslan, *Computational Investigations of Ideal Magnetohydrodynamic Plasmas with Discontinuities*, Dissertation (Univ. Michigan, 1993).
2. N. Aslan and T. Kammash, Developing numerical fluxes with new sonic fix for MHD equations, *J. Comput. Phys.* **133**, 43 (1997).
3. F. Assous, P. Degond, E. Heintze, P. A. Raviart, and J. Segre, On a finite-element method for solving the three-dimensional Maxwell equations, *J. Comput. Phys.* **109**, 222 (1993).
4. D. S. Balsara, Linearized formulation of the Riemann problem for adiabatic and isothermal magnetohydrodynamics, *Astrophys. J. Suppl.* **116**, 119 (1998).
5. D. S. Balsara, Total variation diminishing scheme for adiabatic and isothermal magnetohydrodynamics, *Astrophys. J. Suppl.* **116**, 133 (1998).
6. D. S. Balsara and D. S. Spicer, A staggered mesh algorithm using high order Godunov fluxes to ensure solenoidal magnetic fields in magnetohydrodynamic simulations, *J. Comput. Phys.* **149**, 270 (1999).
7. A. A. Barmin, A. G. Kulikovskiy, and N. V. Pogorelov, Shock-capturing approach and nonevolutionary solutions in magnetohydrodynamics, *J. Comput. Phys.* **126**, 77 (1996).
8. T. J. Barth, Numerical methods for gasdynamic systems on unstructured meshes, in *An Introduction to Recent Developments in Theory and Numerics for Conservation Laws: Proceedings of the International School, Freiburg/Littenweiler, Germany, October 20–24, 1997*, edited by D. Kröner, M. Ohlberger, and C. Rohde, Lecture Notes in Computational Science and Engineering (Springer-Verlag, Berlin, 1999), Vol. 5, p. 195.
9. F. Bezard and B. Despres, An entropic solver for ideal Lagrangian magnetohydrodynamics, *J. Comput. Phys.* **154**, 65 (1999).
10. J. P. Boris, Relativistic plasma simulation—optimization of a hybrid code, in *Proc. Fourth Conf. Num. Sim. Plasmas, Naval Res. Lab., 1971*, pp. 3–67.
11. J. Brackbill, Fluid modeling of magnetized plasmas, *Space Sci. Rev.* **42**, 153 (1985).
12. J. U. Brackbill and D. C. Barnes, Note: The effect of nonzero $\nabla \cdot \mathbf{B}$ on the numerical solution of the magnetohydrodynamic equations, *J. Comput. Phys.* **35**, 426 (1980).
13. S. H. Brecht, J. Lyon, J. A. Fedder, and K. Hain, A simulation study of east–west IMF effects on the magnetosphere, *Geophys. Res. Lett.* **8**, 397 (1981).
14. M. Brio and C. C. Wu, An upwind differencing scheme for the equations of ideal magnetohydrodynamics, *J. Comput. Phys.* **75**, 400 (1988).
15. P. Cargo and G. Gallice, Roe matrices for ideal MHD and systematic construction of Roe matrices for systems of conservation laws, *J. Comput. Phys.* **136**, 446 (1997).
16. W. Dai and P. R. Woodward, An approximate Riemann solver for ideal magnetohydrodynamics, *J. Comput. Phys.* **111**, 354 (1994).
17. W. Dai and P. R. Woodward, A simple Riemann solver and high-order Godunov schemes for hyperbolic systems of conservation laws, *J. Comput. Phys.* **121**, 51 (1995).
18. W. Dai and P. R. Woodward, A simple finite difference scheme for multidimensional magnetohydrodynamical equations, *J. Comput. Phys.* **142**, 331 (1998).
19. A. Dedner, C. Rohde, and M. Wesenberg, A MHD-simulation in solar physics, in *Finite Volumes for Complex Applications. II. Problems and Perspectives*, edited by R. Vilsmeier, F. Benkhaldoun, and D. Hänel (Hermès Sci. Publ., Paris 1999), p. 491.
20. P. Degond, P.-F. Peyrard, G. Russo, and P. Villedieux, Polynomial upwind schemes for hyperbolic systems, *C. R. Acad. Sci. Paris Ser. I, Math.* **328**(6), 479 (1999).

21. C. R. DeVore, Flux-corrected transport techniques for multidimensional compressible magnetohydrodynamics, *J. Comput. Phys.* **92**(1), 142 (1991).
22. C. R. Evans and J. F. Hawley, Simulation of magnetohydrodynamic flows—a constrained transport method, *Astrophys. J.* **332**, 659 (1988).
23. L. C. Evans, *Partial Differential Equations*, Graduate Studies in Mathematics, (Amer. Math. Soc., Providence, RI, 1998), Vol. 19.
24. A. Frank, T. W. Jones, D. Ryu, and J. B. Gaalaas, The magnetohydrodynamic Kelvin–Helmholtz instability: A two-dimensional numerical study, *Astrophys. J.* **460**, 777 (1996).
25. S. K. Godunov, The symmetric form of magnetohydrodynamics equation, *Numer. Methods Mech. Contin. Media* **1**, 26 (1972).
26. R. Holland, Finite-difference solution of Maxwell's equations in generalized nonorthogonal coordinates, *IEEE Trans. Nucl. Sci.* **30**, 4589 (1983).
27. B.-N. Jiang, *The Least-squares Finite Element Method: Theory and Applications in Computational Fluid Dynamics and Electromagnetics*, Scientific Computation (Springer-Verlag, Berlin/Heidelberg, 1998).
28. B.-N. Jiang, J. Wu, and L. A. Povinelli, The origin of spurious solutions in computational electromagnetics, *J. Comput. Phys.* **125**(1), 104 (1996).
29. P. Londrillo and L. Del Zanna, High-order upwind schemes for multidimensional magnetohydrodynamics, *Astrophys. J.* **530**(1), 508 (2000).
30. N. K. Madsen and R. W. Ziolkowski, A three-dimensional modified finite volume technique for Maxwell's equations, *Electromagnetics* **10**, 147 (1990).
31. A. Malagoli, G. Bodo, and R. Rosner, On the nonlinear evolution of magnetohydrodynamic Kelvin–Helmholtz instabilities, *Astrophys. J.* **456**, 708 (1996).
32. B. Marder, A method for incorporating Gauss' law into electromagnetic PIC codes, *J. Comput. Phys.* **68**, 48 (1987).
33. C.-D. Munz, F. Kemm, R. Schneider, and E. Sonnendrücker, Divergence corrections in the numerical simulation of electromagnetic wave propagation, in *Proceedings of the 8th International Conference on Hyperbolic Problems (Magdeburg), 2000*, to appear.
34. C.-D. Munz, P. Omnes, R. Schneider, E. Sonnendrücker, and U. Voss, Divergence correction techniques for Maxwell solvers based on a hyperbolic model, *J. Comput. Phys.* **161**(2), 484 (2000).
35. C.-D. Munz, R. Schneider, E. Sonnendrücker, and U. Voss, Maxwell's equations when the charge conservation is not satisfied, *C. R. Acad. Sci. Paris Ser. I, Math.* **328**, 431 (1999).
36. K. G. Powell, *An Approximate Riemann Solver for Magnetohydrodynamics (That Works in More than One Dimension)*, ICASE-Report 94-24 (NASA CR-194902) (NASA Langley Research Center, Hampton, VA 23681-0001, 8. April 1994).
37. K. G. Powell, P. L. Roe, T. J. Linde, T. I. Gombosi, and D. L. De Zeeuw, A solution-adaptive upwind scheme for ideal magnetohydrodynamics, *J. Comput. Phys.* **154**, 284 (1999).
38. K. G. Powell, P. L. Roe, R. S. Myong, T. Gombosi, and D. De Zeeuw, An upwind scheme for magnetohydrodynamics, in *Numerical Methods for Fluid Dynamics*, edited by K. W. Morton and M. J. Baines (Clarendon, Oxford, 1995), Vol. V, p. 163.
39. D. Ryu, F. Miniati, T. W. Jones, and A. Frank, A divergence-free upwind code for multidimensional magnetohydrodynamic flows, *Astrophys. J.* **509**(1), 244 (1998).
40. G. Starke, Multilevel preconditioning for the time-harmonic Maxwell equations, in *12th Annual Review of Progress in Applied Computational Electromagnetics* (Applied Computational Electromagnetics Society, 1996), p. 630.
41. J. M. Stone and M. L. Norman, ZEUS2D: A radiation magnetohydrodynamics code for astrophysical flows in two space dimensions. II The magnetohydrodynamic algorithms and tests, *Astrophys. J. Suppl.* **80**(2), 791 (1992).
42. A. Taflove, Re-inventing electromagnetics: Supercomputing solution of Maxwell's equations via direct time integration on space grids, Paper 92-0333 (AIAA, 1992).
43. G. Tóth, The $\nabla \cdot B = 0$ constraint in shock-capturing magnetohydrodynamics codes, *J. Comput. Phys.* **161**, 605 (2000).

44. G. Tóth and D. Odstrčil, Comparison of some flux corrected transport and total variation diminishing numerical schemes for hydrodynamic and magnetohydrodynamic problems, *J. Comput. Phys.* **128**, 82 (1996).
45. M. Wesenberg, A note on MHD Riemann solvers, Preprint 35 (Albert-Ludwigs-Universität, Mathematische Fakultät, Freiburg, November 2000).
46. K. S. Yee, Numerical solution of initial boundary value problems involving Maxwell's equations in isotropic media, *IEEE Trans. Antennas Propag.* **14**, 302 (1966).
47. A. L. Zachary and P. Colella, Note: A higher-order Godunov method for the equations of ideal magnetohydrodynamics, *J. Comput. Phys.* **99**, 341 (1992).
48. A. L. Zachary, A. Malagoli, and P. Colella, A higher-order Godunov method for multidimensional ideal magnetohydrodynamics, *SIAM J. Sci. Comput.* **15**(2), 263 (1994).